The Thesis Committee for John Jacob Tatarchuk II
Certifies that this is the approved version of the following thesis:

Comparison of Soft Magnetic Materials Response to Sinusoidal Voltage and Current Excitation

APPROVED BY
SUPERVISING COMMITTEE:

Supervisor:

John A. Pearce

Co-Supervisor:

Aleta T. Wilder

Comparison of Soft Magnetic Materials Response to Sinusoidal Voltage and Current Excitation

by

John Jacob Tatarchuk II, B.E.E.

Thesis

Presented to the Faculty of the Graduate School of

The University of Texas at Austin

in Partial Fulfillment

of the Requirements

for the Degree of

Master of Science in Engineering

The University of Texas at Austin

August 2011

Acknowledgements

I would like to thank Dr. Aleta T. Wilder for her guidance throughout the course of this research and assistance in editing this thesis. I would also like to extend my thanks to Dr. John A. Pearce for providing helpful technical, academic, and literary advice, and for making the PEL available for us to use. Finally, I gratefully acknowledge the support of this research by the U.S. Office of Naval Research under grant N00014-10-1-0559.

John Tatarchuk

Abstract

Comparison of Soft Magnetic Materials Response to Sinusoidal Voltage and Current Excitation

John Jacob Tatarchuk II, M.S.E.

The University of Texas at Austin, 2011

Supervisors: John A. Pearce, Aleta T. Wilder

A pulse hysteresisgraph system was constructed capable outputting current source and voltages source waveforms. MATLAB scripts were created to analyze the collected data.

Three toroidal samples of soft magnetic materials were prepared. Theoretical modeling was done to predict the variation of effective applied magnetic fields inside the toroids from ideal assumptions due to three effects: wire spacing, cylindrical spreading, and eddy current generated fields.

Data was collected under sinusoidal voltage source and sinusoidal current source excitation at 1 kHz. Large differences in core loss were noted especially at higher field excitations. Core loss under sinusoidal current source excitation was found to always be greater than or equal to core loss under sinusoidal voltage source. Normal magnetization curves under sinusoidal current and voltage source excitation were also compared. Significant differences were apparent in the magnetization curves of one sample toroid, and slight differences noted in the curves of the other two samples. Eddy currents were offered as a primary mechanism for the difference in core loss between sinusoidal current source and sinusoidal voltage source. A formula to predict the relative eddy current losses to be expected from an arbitrary, periodic voltage waveform shape is given.

Table of Contents

List of Tables

List of Figures

Chapter 1: Introduction

This thesis examines the behavior differences between voltage source excitation and current source excitation in soft magnetic materials. The three materials characterized are commercial laminates used to build magnetic cores for electromechanical machinery. It is in the winding-core component that the energy conversion form electric to magnetic to mechanical occurs. The understanding of soft magnetic response to excitation fields is critical in moving forward to more efficient, power-dense machines.

As the waveforms driving electromagnetic machinery move to higher and higher frequencies and away from sinusoidal excitations, the understanding of magnetic response at higher frequencies and to non-sinusoidal excitation is becoming more important. At higher frequencies, core loss is an important factor in power consumption, as the number of dynamic hysteresis loops a magnetic material undergoes not only increases (more cycles per second), but loss mechanisms such as eddy current loss increase in magnitude with the increasing rate of change of the excitation. Although difference in sinusoidal voltage source and sinusoidal current source are predicted due to the nonlinear nature of magnetic permeability, this is the first consistent and reliable treatment of this topic.

Testing standards can be unclear as to whether current source or voltage source excitation is to be used to determine a material's magnetic response, or can ignore the frequency dependent effects such as eddy currents on the measured permeability curves of a material. It is important that magnetic behavior under current source or voltage source excitation be modeled with materials data taken under the same excitation method. Additionally, much electromechanical machinery is developed to operate under PWM (pulse width modulation) operation to allow for variable speeds and higher switching efficiencies, which can cause manufacturer's materials data to be even less representative for modeling material response. As a result, those interested in modeling machine behavior through methods such as FEA (finite element analysis) software need improved materials data for the accurate prediction of machine performance and core loss.

The desire to study the differences between magnetic materials response to excitation by various waveform shapes led to the construction of a pulse hysteresisgraph system. To supply the high current levels demanded for rigorous testing of toroidal magnetic samples, two circuits were created. The first is a variant on the class AB push-pull amplifier design, and has a high output impedance capable of outputting current waveforms up to about 15 A. The second is a low output impedance voltage buffer capable of supplying well in excess of 15 A.

Modeling of magnetic behavior was undertaken to understand the validity of assumptions regarding the uniformity of field strength within the samples. Examinations were done of the expected variation in magnetic field due to discrete windings, cylindrical spreading, and eddy current effects.

Finally, data were taken and the results analyzed with interest taken in the dynamic loops, core loss, and normal magnetization curves under both sinusoidal current source and sinusoidal voltage source conditions. Significant differences were found.

Chapter 2: Hysteresisgraph System

Recording dynamic hysteresis loops under trapezoidal, triangular, sinusoidal, sinusoidal with minor loops, and pulsed variations of these waveforms was required as a general research goal. However, commercially available hysteresisgraphs are typically only capable of testing magnetic materials with a specific waveform shape to meet established testing standards. As a commercial solution was unavailable, a prototype hysteresisgraph system capable of measuring the magnetic properties of materials with arbitrarily-shaped current and voltage waveforms had to be constructed.

The approach used to develop a prototype hysteresisgraph system was to use a function generator to create the desired waveform and then amplify or buffer this waveform to create the desired higher-power waveform. Next, the current was measured and recorded as it passed through the primary coil of the sample under test, and simultaneously, the voltage induced on a secondary coil of the sample under test was also recorded. Finally, these data were analyzed to derive the flux density and magnetic field in the sample under test. This system is summarized graphically in Figure 1.

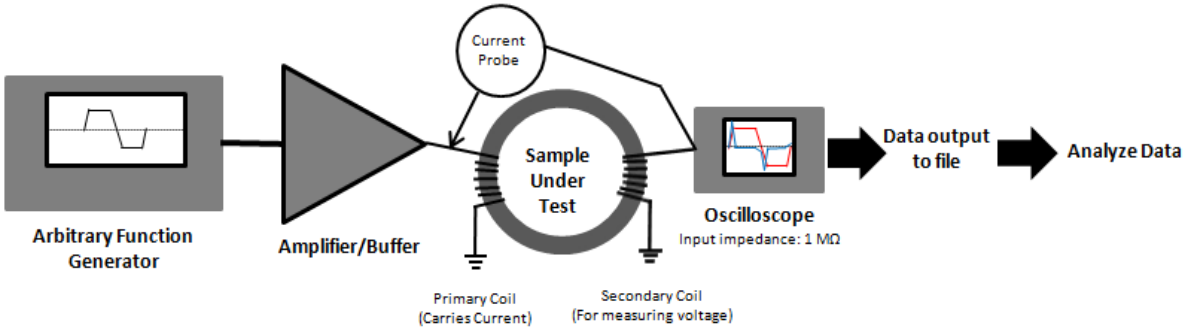

Figure 1: Schematic of Prototype Hysteresisgraph System

Laboratory equipment utilized for the pulse hysteresisgraph system included:

1. Tectronix TCP202 current probe (capable of measuring currents up to 15A)
2. Picoscope 3424 PC oscilloscope
3. Agilent 33521A function generator

4. Two BK Precision 1621A power supplies

All measurements were made in the Process Energetics Laboratory in the CEER building on UT's Pickle Research Campus, and laboratory equipment not on the list above was at times utilized in prototype designs.

Generation of the signal voltage waveform was handled by an Agilent 33521A function generator. Besides the standard waveform shapes found in most function generators, the Agilent 33521A is capable of converting files containing up to 16000 points into an arbitrary waveform shape. Various waveform shapes were tested during the course of this project; only a small number of these are shown in this paper.

2.1 CURRENT AMPLIFIER

The project required the construction of a pulse hysteresisgraph capable of creating pulsed current waveforms with rise and fall times on the order of several tens of microseconds with peak currents approaching 15 A. The samples intended to be driven have inductances in the range of 10-50 μH. Combined with the required dI/dt values in the hundreds of thousands of amps per second, then voltages up to around 15V were anticipated, so it was imperative that the current amplifier have a high cutoff frequency and a very high slew rate.

Early efforts at acquiring the current amplifier required were focused towards finding a suitable and affordable commercial solution. However, commercial amplifiers tended to be low impedance voltage buffers/amplifiers and/or limited by cutoff frequencies of around 20 kHz, obviously intended for the audio region. A Kepco BOP36-12DL amplifier was ordered, but the delivery time of four months prevented its use for this project.

Due to the lack of an available commercial amplifier that met design requirements, the decision was made to construct one. Several possible designs for a prototype amplifier were investigated. The decision was eventually made to build a class AB or similarly-designed amplifier, utilizing BJTs in a "push-pull" type configuration. BJTs were chosen for familiarity and due to their suitability for the task. A conventional push-pull type, class AB

current amplifier was originally considered, such as shown in Figure 2. A variety of resistor values were tested and Figure 2 depicts a typical set of these.

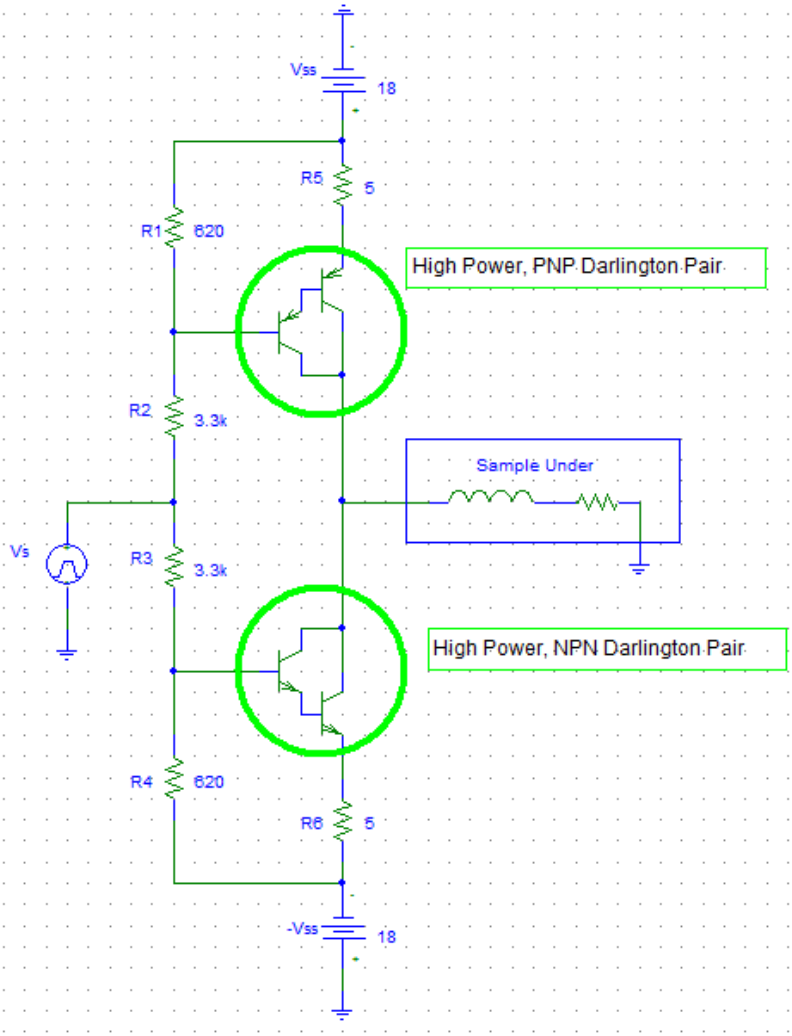

Figure 2: Conventional Class AB push-pull BJT Amplifier

Multiple parallel stages of this design would be combined in order to output the required high-current waveform. However, the basic class AB push-pull amplifier suffers from non-linear gain as the base-emitter voltage varies with larger currents. For BJTs in this configuration, the collector current can be approximated by the following equation:

$$I_c \cong \frac{(V_b - V_{be})}{R_e} \tag{1}$$

where I_c= collector current, V_b= base voltage, V_{be}= base to emitter voltage, and R_e= emitter resistor. This approximation becomes more exact if negligible current is flowing into the base.

Since V_{be} typically has a value around 0.7 volts for a single BJT (and thus, 1.4 volts for a Darlington pair), this circuit acts to convert the voltage waveform present at the base into a current waveform.

For the circuit shown in Figure 2, solving for the collector current on the PNP Darlington, one gets:

$$I_{c,PNP} \cong \frac{\frac{R_1}{R_1 + R_2}(V_{ss} - V_s) - V_{eb}}{R_5} \tag{2}$$

and collector current for the NPN Darlington is found to be:

$$I_{c,NPN} \cong \frac{\frac{R_4}{R_4 + R_3}(V_{ss} + V_s) - V_{be}}{R_6} \tag{3}$$

Since $R_1 = R_4$, $R_2 = R_3$, $R_5 = R_6$, $V_{be} \cong V_{eb}$, and the current through the load is the difference between $I_{c,PNP}$ and $I_{c,NPN}$, then the current through the load is:

$$I_L \cong \frac{-2R_1}{R_5(R_1 + R_2)} V_s \tag{4}$$

where the negative sign represents that a positive input voltage causes the circuit to "pull" current from ground.

In order to maximize the current output of this circuit, several of these stages are placed in parallel, the values of R2 and R5 are minimized, and the value of R1 is maximized.

Unfortunately, however, this amplifier design tends to be inefficient, with large currents drawn through the transistors even when no signal is present. An important characteristic of the class AB amplifier is that it avoids switching any transistors on or off, which prevents "crossover" distortion. All the transistors are always "on", and the output current waveform is created by the difference in the current demands between the PNP and NPN sides of the circuit. So if, as in this case, an amplifier that can output +/- 15 A is required, then at least 7.5 A must be flowing through each PNP/NPN half of the circuit with no signal present. With eight stages, this approaches 1 A per stage. However, with sufficient heat-sinking, high power solid state electronics, and the ability to add more stages in parallel rather easily if necessary, then this can be quite acceptable.

An additional problem arises due to the fact that V_{be} will vary as collector/emitter current increases or decreases. An example of this nonlinearity is depicted graphically in Figure 3 which is from Motorola's datasheet for the TIP 121 (an NPN Darling used in the eventual final design):[1]

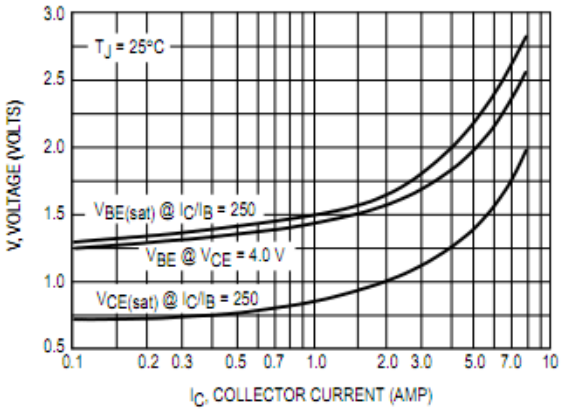

Figure 3: TIP 120 Series Transistor Voltages at Various Collector Currents

[1] Motorola Literature Distribution. *TIP120 TIP121 TIP122 TIP125 TIP126 TIP127, Plastic Medium-Power Complementary Silicon Transistors, Motorola Semiconductor Technical Data* [Online]. Available: http://www.datasheetcatalog.org/datasheet/motorola/TIP127.pdf

Figure 3 shows that as collector current increases, V_{be} can also be expected to rise by a significant amount. While the use of multiple stages reduces the amount of variation in V_{be} that should be expected by dividing the total current amongst several devices, Figure 3 indicates that the variation is still undesirable as it reduces linearity. As more current is output, V_{be} becomes larger, causing the amplifier to output noticeably less current than a linear amplifier would. Due to this issue, an op-amp was to the circuit in the configuration shown in Figure 4 was constructed and tested.

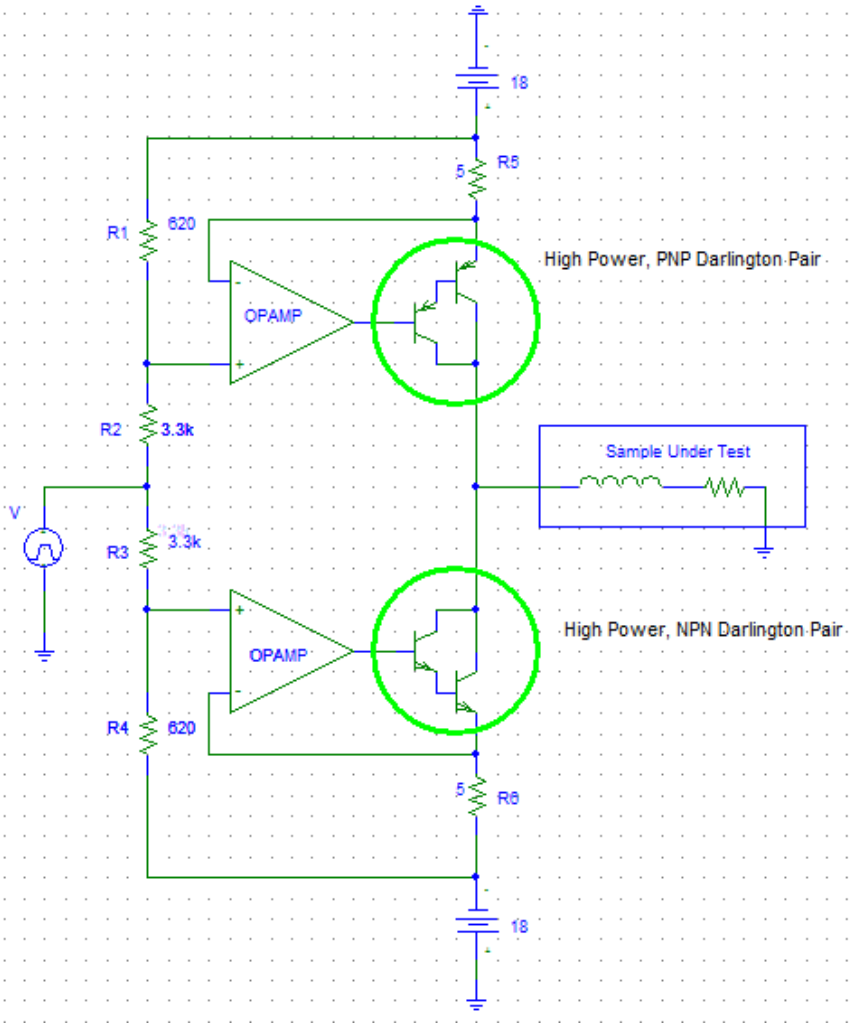

Figure 4: Push-Pull Amplifier with Op-Amp Biasing of Transistors

In the configuration shown in Figure 4, the op-amps force the circuit node between R5 and the PNP emitter and the node to between R6 and the NPN emitter to be at the same voltage as the nodes between R1 and R2, and R3 and R4. This eliminates the V_{be} and V_{eb} terms from equations 1 through 3. Additionally, since op-amps have a very high input resistance, the approximation that negligible current flows into the base (which is assumed for equations 1 through 4) becomes valid.

The uA741 op-amp IC (a large number of which were immediately available in the Process Energetics lab) was initially tested in this configuration, and BJT Darlington pair transistors of the TIP 120 series were used. However, the uA741 is limited to a slew rate of around 0.5 MV/s.[2] As a result, the amplifier proved incapable of driving the sample through rapid changes in current in the unsaturated region of a sample's normal magnetization curve. It was estimated that an op-amp with a slew rate of at least 5-10 MV/s was required, and the LF353 op-amp was chosen. The particular LF353 that was purchased was manufactured by STMicroelectronics, and was specified to a slew rate of 16 MV/s. [3]

While the uA741 proved stable but unable to slew fast enough to maintain the desired current waveform, the LF353, when used in the same configuration shown in Figure 4, proved very unstable, which was not unsurprising in retrospect. A very fast op-amp with a high slew rate will respond faster than the transistor switching time. This creates a phase delay in the feedback loop that causes the circuit to oscillate severely. After experimenting with several different configurations in attempts to limit the slew rate, it was decided that the effects of a slightly variable V_{be} and slight amplifier nonlinearity were acceptable compared to the time it would take to create and test a more linear amplifier design.

A modified op-amp based approach to biasing the Darlington pairs was adopted instead. As previously mentioned, the class AB design is fairly inefficient. Because of the amount of adjustment and optimization during the testing of the various amplifier designs, it

---

[2] STMicroelectronics. (2001). *UA741, General Purpose Single Operational Amplifier* [Online]. Available: http://www.datasheetcatalog.org/datasheet/stmicroelectronics/5304.pdf

[3] STMicroelectronics. (2010). *LF253, LF353, Wide bandwidth dual JFET operational amplifiers* [Online]. Available: http://www.st.com/internet/com/TECHNICAL_RESOURCES/TECHNICAL_LITERATURE/DATASHEET/CD00000454.pdf

was considered useful to make an amplifier that was highly adjustable and could change configurations easily. The amplifier configuration shown in Figure 5 was thus constructed.

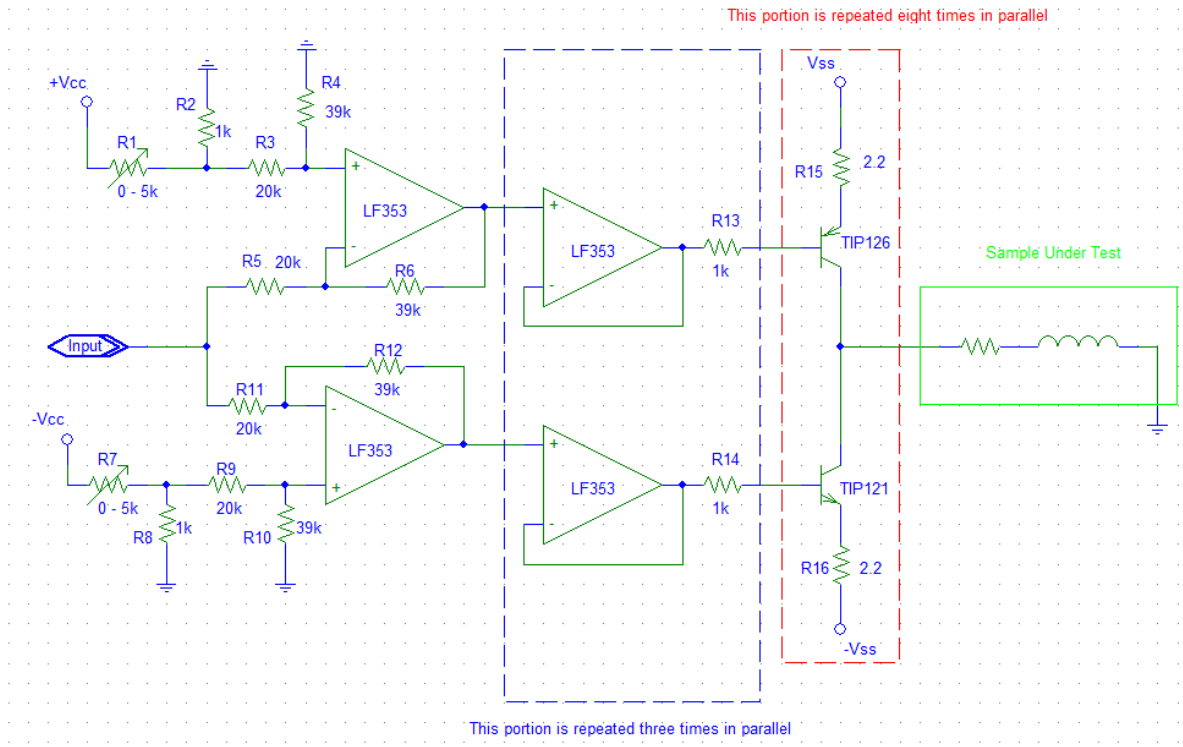

Figure 5: Final Current Amplifier Design

The design shown in Figure 5 biases the transistors with op-amp subtractor circuits that offer several advantages over the usual resistive bias network of a class AB amplifier. First, they allow the power consumption the in amplifier to be reduced when it is being used at lower power. Further, incorporating op-amp subtractor circuits allows an offset current to be added or subtracted, or the signal to be balanced, by adjusting potentiometers with a screwdriver. The voltage-to-current gain can also be adjusted easily by changing the value of R6 and R12. Additionally, this design was constructed on a breadboard, allowing the biasing configuration to be easily changed.

Considering only the circuit that sets the base voltage for the PNP type TIP126, the voltage on the base of the transistor can be derived. Using ideal op-amp assumptions of $v_+ = v_-$ and $i_+ = i_- = 0$, where v_+, i_+ are the voltage and current on the positive input

terminal and v_-, i_- are the voltage and current on the negative input terminal of the op-amp, then voltage on the positive input terminal of the op-amp is exactly:

$$v_+ = V_{cc} \cdot \frac{R_2 \| (R_3 + R_4)}{R_1 + R_2 \| (R_3 + R_4)} \cdot \frac{R_4}{R_3 + R_4} \tag{5}$$

which, because $R_2 \ll (R_3 + R_4)$, is approximately:

$$v_+ \cong V_{cc} \cdot \frac{R_2}{R_1 + R_2} \cdot \frac{R_4}{R_3 + R_4} \tag{6}$$

Again using ideal op-amp assumptions, the voltage at the negative terminal, v_-, must be the same voltage as v_+, and the current through resistor R_6, i_{R_6}, must be the same as the current through resistor R_5. Thus, the current through resistor R_6 is determined by v_+, R_5, and the input signal voltage, V_{in} as:

$$i_{R_6} = \frac{V_{in} - v_+}{R_5} \tag{7}$$

The output voltage of the op-amp now becomes:

$$v_o = v_+ - i_{R_6} R_6 = v_+ - \frac{V_{in} - v_+}{R_5} \tag{8}$$

where v_o is the voltage on the output terminal of the op-amp. Using the approximation for v_+ (equation 6), v_o becomes:

$$v_o \cong \frac{R_6}{R_5}\left[V_{cc} \cdot \frac{R_2}{R_1 + R_2} \cdot \frac{R_4}{R_3 + R_4} \cdot \left(1 + \frac{R_5}{R_6}\right) - V_{in}\right] \tag{9}$$

This output voltage passes through a protective buffer circuit for each stage that provides a degree of isolation and prevents excessive current from being drawn from the op-amp. Since

the input resistance to the PNP BJT Darlington pair is much greater than the 1 kΩ resistor between the output of the buffer and the base, the output voltage of the top op-amp circuit in Figure 5 is then the base voltage of the PNP:

$$V_{b,PNP} \cong \frac{R_6}{R_5}\left[V_{cc} \cdot \frac{R_2}{R_1 + R_2} \cdot \frac{R_4}{R_3 + R_4} \cdot \left(1 + \frac{R_5}{R_6}\right) - V_{in}\right] \tag{10}$$

Calculations for the bottom op-amp circuit that generates the base voltage for the NPN Darlington pair are identical except for a negative sign in front of V_{cc}, and the potentiometer R_7, which can be a different value of resistance than the value R_1 is set to. All other resistor values in the bottom op-amp circuit are the same as their corresponding values in the top op-amp circuit, and $V_{b,PNP}$ can be calculated as:

$$V_{b,NPN} \cong -\frac{R_6}{R_5}\left[V_{cc} \cdot \frac{R_2}{R_7 + R_2} \cdot \frac{R_4}{R_3 + R_4} \cdot \left(1 + \frac{R_5}{R_6}\right) + V_{in}\right] \tag{11}$$

To solve for the current in the load, it is important to consider that the Darlington pair configuration has a very high value of current gain. Thus, the current through the emitter can be assumed to be the same as the current through the collector. For the PNP Darlington, the current flowing into the emitter is:

$$I_{e,PNP} = \frac{V_{ss} - V_{b,PNP} - V_{eb}}{R_e} \tag{12}$$

and for the NPN Darlington, the current flowing into the emitter is:

$$I_{e,NPN} = \frac{V_{b,NPN} - V_{be} + V_{ss}}{R_e} \tag{13}$$

The current flowing into the load is the difference of equations 12 and 13. Subtracting these two equations and substituting in the values of $V_{b,PNP}$ and $V_{b,NPN}$ found in equations 10 and 11, the load current for a single stage is:

$$I_L = \frac{1}{R_e} \cdot \left[\frac{R_6}{R_5} \cdot \frac{R_4}{R_3 + R_4} \cdot \left(1 + \frac{R_5}{R_6}\right) \cdot \left(\frac{R_2}{R_7 + R_2} - \frac{R_2}{R_1 + R_2} \right) \cdot V_{cc} + \frac{2R_6}{R_5} \cdot V_{in} - V_{eb,PNP} - V_{be,NPN} \right] \quad (14)$$

If $V_{eb,PNP} = V_{be,NPN}$ and $R_7 = R_1$, then the predicted load current for a single stage simplifies to:

$$I_L = \frac{2R_6}{R_5 R_e} \cdot V_{in} \quad (15)$$

Even though this design lacks a feedback loop on the op-amps connected to the TIP 120 bases, the inclusion of the 1 kΩ stabilizing resistor R_s between the buffer amplifier and the base of each transistor was necessary to keep the amplifier from oscillating. With the very high input resistances of the TIP 120s, this stabilizing resistor does not noticeably affect the output current waveform's expected shape as the voltage drop across R_s is minimal.

A single stage was built and tested to this design. Eight stages of TIP121/126s were subsequently connected, and three LF353 buffers were used to buffer the voltage for these transistors, as indicated in Figure 5.

Two BK Precision 1692 switching DC power supplies were purchased and hooked in series to supply the TIP120s with the high current they demand. The voltage was adjusted on each power supply to 12 volts to set the value of V_{ss}. The power supplies used for the LF353 op-amp networks are the two BK Precision 1621A power supplies, connected in series and set for 15 volts each. The series connection points of the two sets of power supplies are wired together to ensure that they share a common ground.

While this amplifier was adequate to fulfill project requirements, a few issues remain. First, the output current will slowly "wander" through a ~10mA range as thermal effects cause the base to emitter voltage of the transistors to slowly change. Secondly, the approximation that $V_{eb,PNP} = V_{be,NPN}$ becomes less valid as the difference between the amounts of current that the two transistors conduct increases. These issues can be partially solved by connecting either R_5 or R_{11} to ground rather than the input signal. In this configuration, only the PNP or NPN transistors will act as an amplifier. The other transistors are used to add an offset current (by adjusting the potentiometer R_1or R_7 as required) that will bring the average current to the value desired. While the amplifier in this configuration will usually output a cleaner waveform, it is only half as efficient, and can only output half as much peak current.

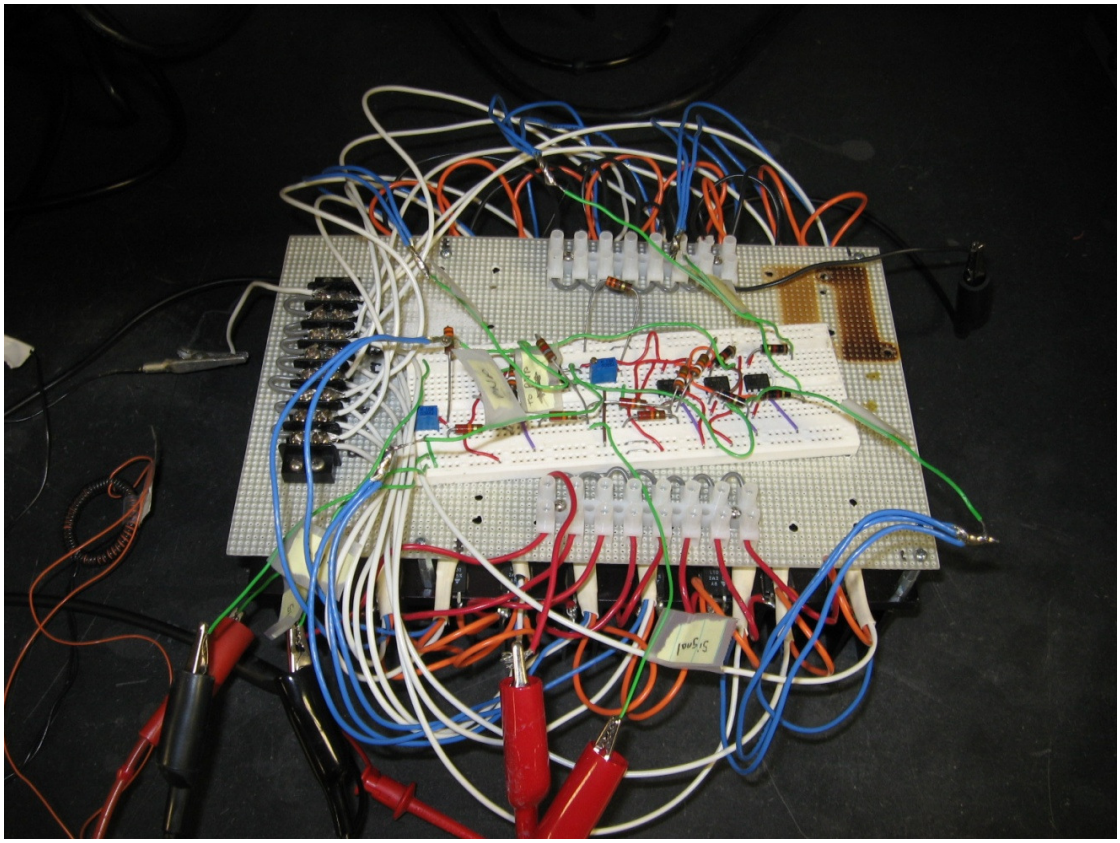

Figure 6: Current Amplifier

Figure 7, shows output waveforms of the current amplifier operating in its normal operating mode (where all the transistors are being used to amplify the signal).

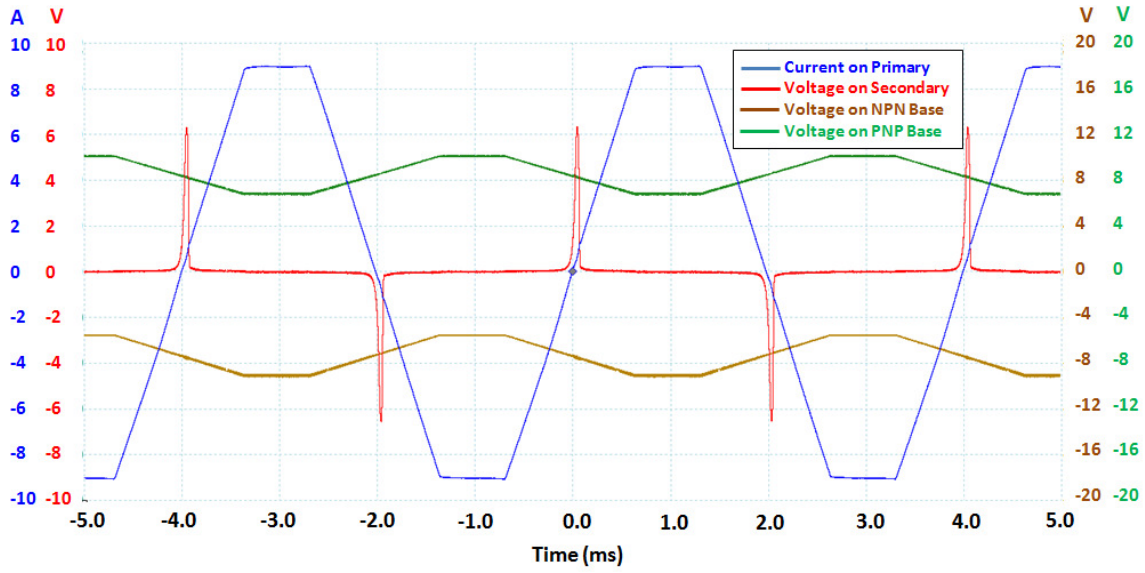

Figure 7: Current Amplifier Example Output

2.2 VOLTAGE BUFFER

While the initial requirement for the hysteresisgraph was to output current source waveforms, interest grew to measure sample response to voltage source waveforms as well. Sinusoidal voltage excitation is the more common waveform for powering electromagnetic machinery. The Kepco amplifier that was received is inadequate for generating the desired voltage waveforms, as a load impedance of a few hundred ohms was recommended by the manual while in voltage source mode. Thus, a voltage amplifier with a sufficiently low output impedance to maintain the desired voltage waveform shape was designed.

As the Agilent 33521A function generator is able to output up to +/- 10 V, it was deemed unnecessary to actually amplify voltage. A simple voltage buffer with a very low output impedance, implemented with op-amp circuits, could meet performance requirements. This low impedance voltage buffer requires op-amps with the following characteristics:

1. High slew rate (preferably 5MV/s or better)
2. High output current (total output current of the buffer should be >10A

3. Able to operate with +/- 10 to 15 volt power supplies
4. Gain Bandwidth (GBW) Product greater than ~100kHz

The OPA 544T op-amp was selected for this low impedance voltage buffer. The datasheet for the OPA 544T [4] indicates that this op-amp fulfills the listed requirements when several stages are combined. [5]

The amplifier required significant heat dissipation in order to prevent thermal damage. The safe operating area, as defined in Figure 2 of the TI data sheet, is shown in Figure 8.

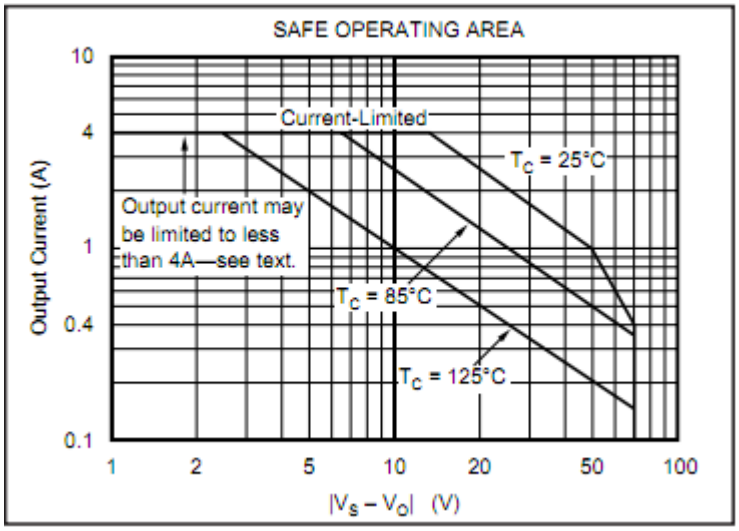

Figure 8: OPA 544T Safe Operating Area [4]

Figure 8 demonstrates the sensitivity of the amplifier's maximum safe output current to its junction temperature. The expression $|V_s - V_o|$ is the magnitude of the difference between the power supply voltage and the output voltage, applicable to the conducting transistor within the op-amp. The most extreme difference between the magnitude of the power supply voltage (V_s) and the output voltage (V_o) is limited to around 20V using the same BK Precision 1692 DC power supplies that the current amplifier uses, configured to supply +/- 12 V. If

[4] Texas Instruments. (2010, August 2). *OPA544, High-Voltage, High-Current, Operational Amplifier* [Online]. Available: http://focus.ti.com/lit/ds/symlink/opa544.pdf

[5] Slew rate of 8MV/s, an output current of up to 4A, required power supply voltages of +/- 10 V to +/- 35V, and a GBW product of 1.4MHz

cooled to 25° C, the maximum safe output current should be in the neighborhood of 2.3 A at this voltage limit. However, it is unlikely that the buffer would operate in this region. Even if it did, it would only spend a very small amount of time there. A more likely limit would be to consider that the maximum $|V_s - V_o|$ for the buffer will be 12 V, and thus, the safe operating current would be 4 A. A design with six stages was optimal to ensure that the buffer is limited to the safe operation regions when outputting up to 15 A.

In the first attempt to create a stage, it was discovered that the circuit was unstable with no circuit components other than the op-amp itself. Adding more parallel stages just increased the instability. In addition, the positive terminal of the op-amp was grounded through a resistor so that when the function generator was disconnected, the input terminal was not allowed to float.

To stabilize the op-amps, decoupling capacitors were added to help remove the power supply ripple, and a 1.5 Ω resistor was added in the feedback loop to help improve stability. The resulting stages proved stable both individually and in parallel during subsequent testing. Figure 9 shows the final design configuration.

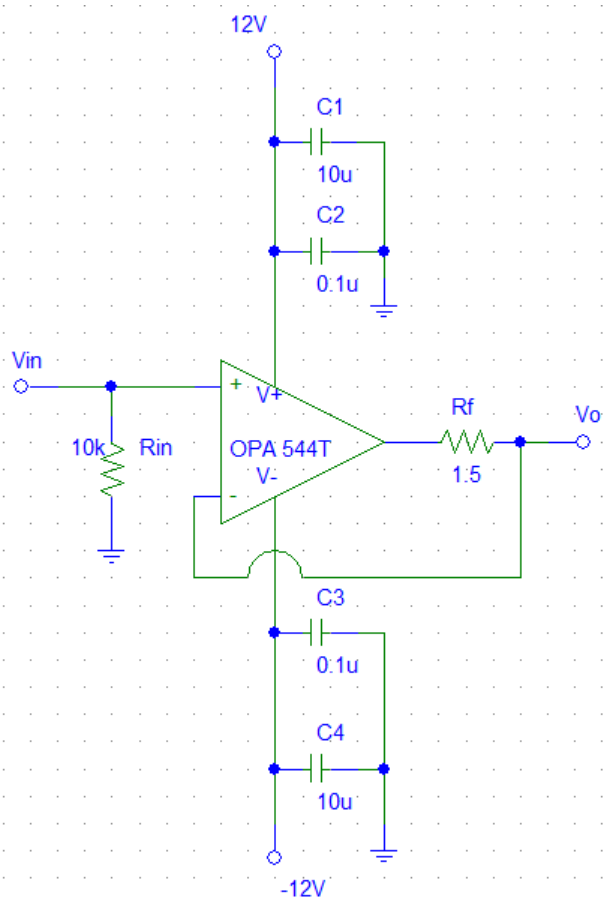

Figure 9: Low Impedance Voltage Buffer

While R_f is of vital importance in stabilizing the op-amp, it does limit the maximum voltage at higher currents where significant voltage can be dropped across this resistor. With six stages, at 15 A (the maximum output current the buffer is intended to supply), 3.75 V will be dropped across this resistance. Under these load conditions, and when being supplied by +/-12 V (so that the maximum voltage output of the op-amp will be +/-10 V), the output voltage will be limited to +/- 6.25 V. However, the toroid samples studied in this research approach saturation with 2 A of current, and at current above this, their impedance drops significantly. Because of this, the voltage drop across the toroid samples at high currents is low, and at 15 A, 6.25 V is never required.

Testing of the low impedance voltage demonstrates stable performance and the ability of the voltage buffer to reproduce the input waveform with very low levels of distortion. Figure 10 shows an example output from this buffer.

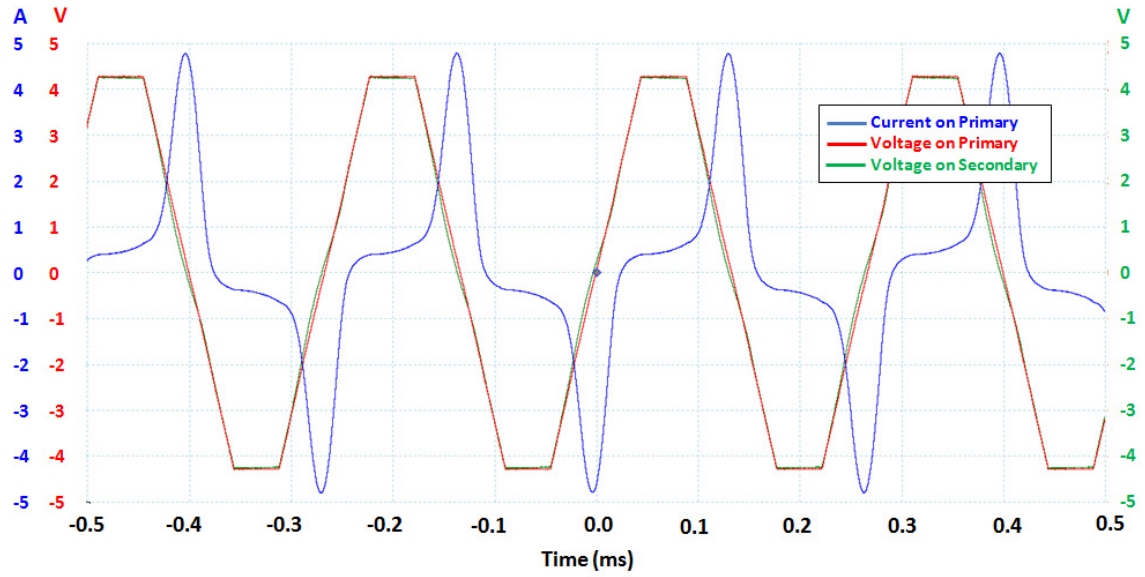

Figure 10: Voltage Buffer Output Waveform Examples

2.3 MATLAB Data Analysis Methods

The Picoscope was configured to collect measurements of the current through the primary coil and the voltage across the secondary coil. Data collected from the Picoscope is saved to text files that are tab-delimited. MATLAB m-files were designed and created to read these text files and automatically generate dynamic hysteresis loops plotted with respect to the applied magnetizing field, **H**, and the spatial average flux density induced in the material, **B**. A more detailed explanation of one of these MATLAB scripts is given in this section.

Several dozen different MATLAB scripts/functions were created in support of this project. Most were minor variations or evolutions upon previous scripts. The script that produced most of the graphs in this paper uses the procedure described in this section for generating dynamic hysteresis loops. The MATLAB script itself is included in Appendix A.

The Picoscope generates text files containing tens of thousands of samples of time, primary current (sensed as voltage), and secondary voltage. The MATLAB script creates a

function that can be called from the main MATLAB interface that reads in and formats this data into three MATLAB matrices. Faraday's Law is used to generate the first estimation of the flux density in the toroid sample, by integrating the voltage on the secondary coil over time (see Chapter 3). The magnetic field is easily found by applying Ampere's Circuital law to the toroid geometry and current waveform, and assuming uniform flux density (see Chapter 3). The MATLAB function now has an initial estimate of magnetic flux density **B**, and applied magnetic field **H**.

An interesting problem is often observed when a dynamic hysteresis loop is plotted. The integrated voltage, representative of flux, may be seen to continuously increase or decrease, causing plotted dynamic hysteresis loops to slowly "spiral" up or down, instead of retracing the original loop. This is seen to happen well into the sinusoidal steady state region. Since the flux density **B** is proportional to the integral of the voltage on the secondary coil, this equates into a DC offset voltage on the secondary coil, almost always less than 1 mV. This offset voltage can often appear to increase in magnitude as the magnitude of the current excitation is increased. To produce cleaner dynamic hysteresis loops, a temporary solution of subtracting or adding an appropriate offset voltage to cancel out the effect of the observed distortion was applied until a proper explanation for the phenomenon could be found.

No explanation was found within theory to explain this DC offset voltage. For example, it cannot be flux related, because a DC offset voltage would represent a continuously increasing or decreasing flux, and all measurements were taken well after transients should have died out. Furthermore, this offset voltage was found to be inconsistent between different measurement sessions and measuring devices. Thus it was concluded that it was due to some phenomenon that was not material-related, and most likely not magnetic materials related either. It is thought to represent some kind of offset or inaccuracy within the measuring oscilloscope itself.

The temporary solution of cancelling out the effect of the offset voltage with an equal and opposite correction voltage became the permanent solution. This was considered satisfactory as the apparent offset voltage was a small effect that made little impact on any

single dynamic hysteresis loop other than making the starting and ending flux densities slightly different. See Figure 11 below for an extreme example of the effect of offset voltage and the same loop with this offset voltage removed.

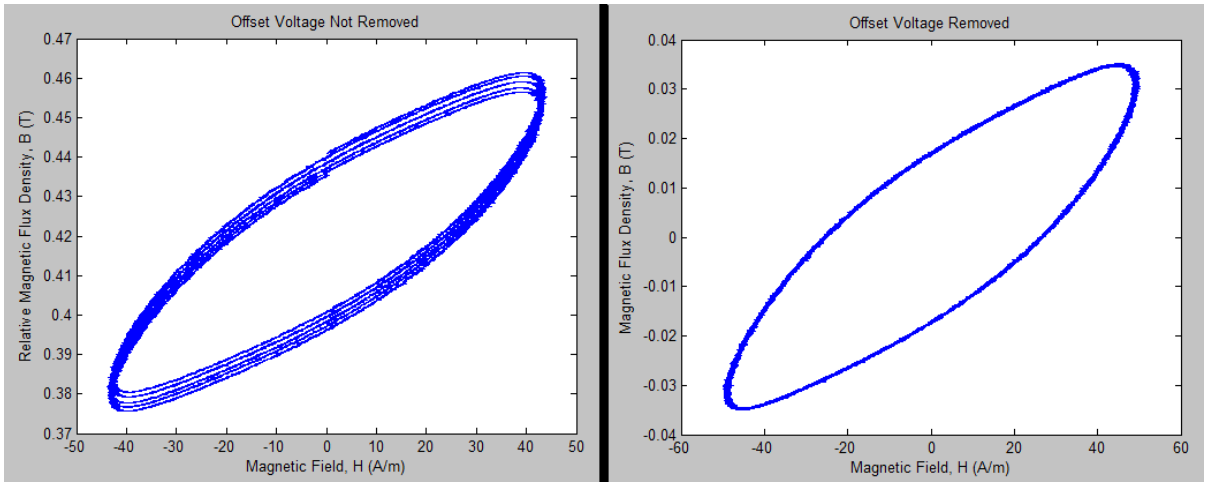

Figure 11: Hysteresis Loops: left) with offset voltage; right) with offset voltage removed.

The MATLAB function that plots the **B** and **H** points on a dynamic hysteresis loop must either take manual input to find a DC voltage value to cancel out the offset voltage, or find the correct counter-offset value automatically. The final iterations of the MATLAB scripts used to generate these graphs were programmed to automatically remove the offset voltage. The automatic offset removal first recognizes a single loop, and then establishes counter-offset voltage value necessary to make the end points of the loop identical. This gives an initial estimate that the MATLAB function can use to step through a range of counter-offset voltage values until the best correlation between all the loops plotted was obtained. In other words, the MATLAB function finds the value of voltage that needs to be added to all samples to best make all loops line up on top of each other.

With the offset removed, final plots of the data can be made, and the core loss is calculated. Additionally, another text file is generated containing core loss data and the datum points defining the dynamic hysteresis loop.

Chapter 3: Theoretical Models

This research required careful study and understanding of magnetic effects within the toroid samples. In addition, to more precisely determine the different magnetic effects, the toroids had to be precisely characterized, and both approximate and full solutions to magnetic behavior had to be determined. In particular, the variation in applied magnetic field (**H**) due to the effects of discrete windings, cylindrical spreading, and eddy current fields was studied.

3.1 Basic Core Loss Mechanisms and Terminology

3.1.1 Core Loss

In electromechanical machinery, two primary mechanisms are used to explain most losses within magnetic materials. The first is known as *hysteresis loss*: loss resulting from the magnetization of the material itself. The amount of energy loss per cycle associated with this phenomenon is constant with respect to frequency. Thus, power lost due to hysteresis loss is a function the frequency at which this the path along the magnetization curve is transversed.

The second loss mechanism is known as *eddy current* loss, and represents resistive heating of core material by induced currents. These currents are proportional to the time rate of change of the flux, which is in turn proportional to the frequency of oscillation. As a result, the amount of power lost due to eddy currents is proportional to the excitation frequency squared.

Together, the two losses make up for the majority of magnetic losses in electromagnetic machinery, and are loosely lumped together as *core loss*. [1]

3.1.2 Normal Magnetization Curves

A plot of the magnetic flux density (**B**) versus applied magnetic field (**H**) for a material is known as a *normal magnetization curve*. Often, the free-space component of **B** is subtracted, but in the work presented in this paper, this was not done as the free space component was negligible compared to the materials component. Where there is significant hysteresis loss, then the normal magnetization curve will typically follow the maximum **B** or maximum **H** points (the two usually reach their max values near or at the same point) on a series of hysteresis loops.

Two prominent features of many normal magnetization curves are referenced in the paper. The first is the *linear region*, where **B** is a linear function of **H**. The second is the *knee*, the region of the curve where the linear relationship breaks down and the material starts approaching saturation. A plot of a normal magnetization curve with these two features labeled is shown in Figure 12.

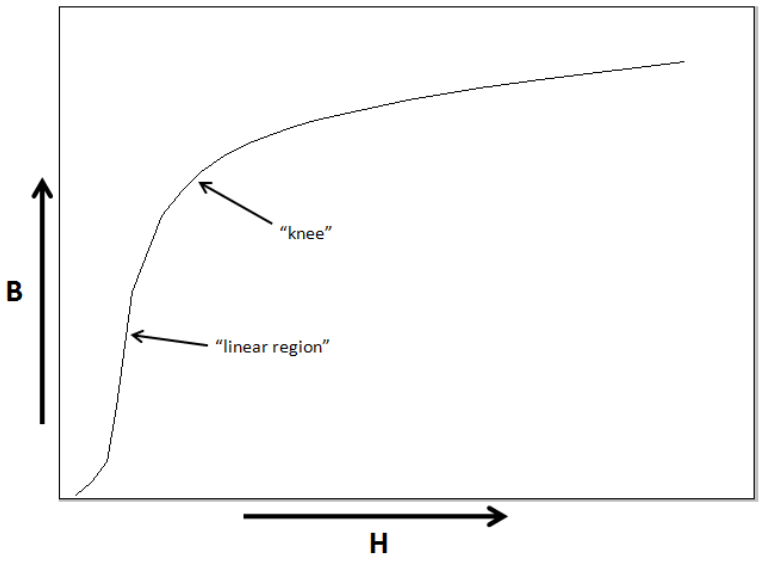

Figure 12: The Linear Region and Knee of a Normal Magnetization Curve

3.2 TOROID PARAMETERS

Sample toroids of Hiperco50 HS (#00058), GF Iron (#00042), and Cogent Sura (#00058) were studied to compare the materials-dependent effects of different magnetizing waveforms. The nominal compositions and some properties for these materials are listed in Table 1.

All three sample toroids were built from commercial, non-oriented magnetic alloy strip. Multiple rings were laser cut from each strip and then annealed in an inert atmosphere per manufacturers' recommended procedures. The rings were stacked with an intervening layer of insulating paper. The orientations of the rings with respect to the strip rolling direction were random. The laminate stack was then wrapped with electrical tape and wound with two wire coils. Varnish-coated magnet wire was used for the primary coil for toroid sample #00058, with PTFE-coated, 20 to 24 gauge, stranded copper wire used for the other primary coils, and for the secondary coils. Both primary and secondary windings are uniformly distributed along the circumference of the toroids.

The toroid samples used in this research were very similar in size, and used between six and nine laminate stacks. With all laminates stacked together, the toroids have a rectangular cross section of about 2.8 mm in the laminate surface plane, by about 0.9mm in the laminate normal plane. Figure 13 assigns the variables to toroid geometry to be used throughout this paper, and Table 2 gives the values of the variables for each of the three toroid samples studied.

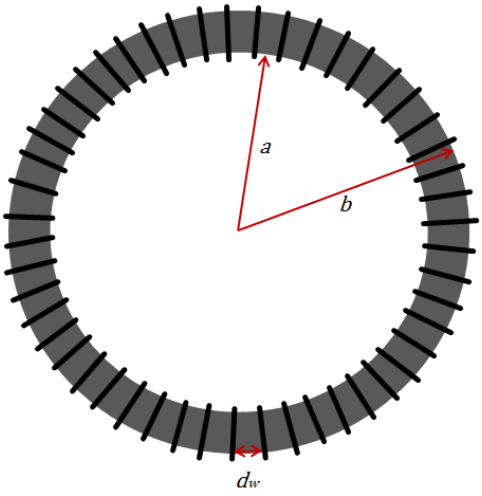

a, inner radius
b, outer radius
r_o, average radius, ($r_o = \frac{a+b}{2}$)
d_w, Wire spacing
w, width of toroid ($w = b - a$)
n_{lam}, number of laminations
h, height/thickness of each lamination

Figure 13: Toroid Geometry

Variations in material composition and processing effect magnetic behavior. It is important to also know the electrical resistivity of each magnetic material so that calculations of eddy current effects can be made. Tables 1 and 2 give values of the pertinent parameters.

Material Parameters			
Toroid Name	#00028	#00042	#00058
Material Name	Hiperco 50	GF Iron	Cogent Sura
Composition (%)	49.19 Fe, 48.75 Co, 1.90 V, 0.05 Si, 0.05 Mn, 0.05 Nb, 0.01 C	99.5 Fe	96.6 Fe, 3.0 Si, 0.4 Al
Manufacturer	Carpenter Technology	--	Cogent Power, Inc.
Annealing	UT Annealed	UT Annealed	UT Annealed
Lamination Thickness (spec) (mm)	0.15	0.099	0.13
Lamination Thickness (measured) (mm) (h)	0.14	0.099	0.13
Lamination Coating	None	None	Native oxide
Density (kg/m³)	8120	7860	7650
Resistivity (Ω-m)	0.41e-6	0.13e-6	0.52e-6

Table 1: Toroid Material Parameters

Toroid Properties			
Toroid Name	#00028	#00042	#00058
Number of Turns, N	57	44	50
Number of Laminations	6	9	7
Total thickness (Number of Laminations X Thickness of Lamination) (mm)	0. 91	0.89	0.89
Outside Radius, b (m)	0.019025	0.019051	0.019051
Inside Radius, a (m)	0.016205	0.016194	0.016194
Average Radius, r_o(m)	0.017615	0.017622	0.017622
Primary coil wire diameter, including insulation (m)	0.001	0.0015	0.001
Total Toroid height (including wire) (m)	0.0049	0.0061	0.005

Table 2: Toroid Physical Dimensions and Parameters

3.3 IDEAL TOROID

The induced voltage on a coil through which flux Φ passes is known through Faraday's law to be:

$$v(t) = -N\frac{d\Phi}{dt} \tag{16}$$

where N is the number of turns in the coil. From this it can be determined that the instantaneous spatial average of flux density inside a coil at any point in time *t* is:

$$B(t) = \frac{1}{NA}\int_{t_0}^{t} v(t)dt + B_r \tag{17}$$

where B_r is the spatial average of the remnance flux density (the flux density initially present at time t_0), $v(t)$ is the voltage across the coil, A is the effective cross-sectional area of the toroid and N is the number of turns. All three toroid samples used in this paper have a secondary winding with the same number of turns as the primary winding (a 1:1 turns ratio). This results in the flux linkage of the primary being equal to the flux linkage of the secondary.

While exciting the primary coil of a toroid with the desired waveform, the voltage on the secondary coil (connected to a high impedance load such as the 1MΩ input of the Picoscope) can be measured to determine the voltage induced by the changing magnetic flux. MATLAB is used to integrate this voltage and to find the flux density (as described in Chapter 2.3).

Calculating the loss due to magnetic effects under repetitive cycling is fairly straightforward. The instantaneous power flowing into a circuit is the product of the voltage across a circuit times the current flowing into a circuit, as given below.

$$P_{ins}(t) = v(t) \cdot i(t) \tag{18}$$

For a periodic waveform, the total energy lost would be equation 18 integrated over one period, *T*. Considering the 1:1 turns ratio of all three toroids studied, and the toroidal geometry variables defined in Figure 13, the energy loss W due to magnetic effects per cycle per unit volume is given by:

$$W = \frac{1}{2\pi r_o A}\int_0^T i_1(t)\, v_2(t) dt \tag{19}$$

where $i_1(t)$ is the current on the primary and $v_2(t)$ is the voltage on the secondary.

The magnetic field within the toroid can be determined by applying Ampere's Circuital Law:

$$\oint_C \vec{H} \cdot \overrightarrow{dL} = I_{inc} \tag{20}$$

where I_{inc} is equal to NI, and I is equal to the current through the coil. The **H** field in the $\overrightarrow{dL}$ direction integrates into the common expression for the magnetic field within a toroid, given as:

$$H = \frac{NI}{2\pi r_0} \tag{21}$$

3.4 Deviations From Ideal Assumptions

It is important to understand how much the magnetic field and flux within the toroid deviates from ideal assumptions. There are three main assumptions concerning the equations for the ideal toriod given above:

1) The current through the toroid coil can approximated by uniform sheet current;
2) The magnetic field is uniform with respect to radius;
3) The magnetic field component due to eddy current generation is negligible compared to the excitation field strength.

3.4.1 Variation Due to Line Currents

The ideal assumption given in equation 21 assumes that the current is created by an ideal sheet current along the surfaces of the toroid. In reality, discrete wire turns are used. While the average value of the magnetic field remains the same as given by Ampere's circuital law, regions of the magnetic material that are closer to a wire are more strongly excited than regions that are more distant. Equation 21 is only considered valid beyond a depth of two times the wire spacing into the coil. [2]

To assess the influence of this approximation, the effects of using wire instead of an ideal sheet current was estimated. A method to calculate the actual magnetic field would be to apply the Biot-Savart law:

$$\vec{H}(r) = \int_L \frac{I\overrightarrow{dL} \times \widehat{a_R}}{4\pi\left|\vec{R}\right|^2} \tag{22}$$

where $\vec{H}(r)$ is the magnetic field at a specific point in 3D space, I is the current on the wire, $\overrightarrow{dL}$ is the differential length element, $\vec{R}$ is the vector from $\overrightarrow{dL}$ to r, and $\widehat{a_R}$ is the unit vector that points in $\vec{R}$.

Equation 22, when applied mathematically to various toroid geometries, can require tedious solutions to solve the integral. [3] For a useful estimate of this effect rather than an

exact solution, equation 22 was solved analytically with MATLAB as described in the following section.

3.4.1.1 MATLAB Simulation of Magnetic Field from Line Currents Approximating a Coil

A MATLAB simulation was created to solve Biot-Savart's Law for a representative toroid geometry. The following assumptions were made in the MATLAB simulation:

1. The skin effect on the wire is negligible, and the wire can be treated as an ideal line current.
2. Eddy current effects and variations of magnetic field with toroid radius are ignored
3. The toroid will be treated as a long rectangular bar (radius goes to infinity)

As this is a simulation of nothing more than the strength of the exciting magnetic field, and the effects of eddy currents and variation of magnetic field with radius are excluded, the toroid geometry is only important in defining the areas where magnetic field values will be calculated and displayed. The magnetic field was calculated for a single unit cell of the toroid, approximately based on toroid sample #00028 dimensions. In the coordinate system defined in Figure 14, a unit cell is defined as:

- Length (z axis, points in toroid rotational, or φ direction) $\stackrel{\text{def}}{=} \tau = \frac{2\pi r_o}{N}$ =1.94mm
- Width (x axis, points in opposite direction of toroid radial direction) = 3 mm
- Height(y axis, points in toroid axial direction) = 1 mm

The height of the toroid (axial direction), where the laminates stack up to be a total of about 1 mm thick, is 5 mm including the wire wrapping. This suggests that to replace the 1 mm thick wire with an ideal line current requires placing the line current 1.5 mm away from the surface of the simulated toroid domain. Thus, using the coordinate system defined in Figure 14, the simulated toroid winding is rectangular and has dimensions of 6 mm (in x direction) by 4 mm (in y direction), and makes one complete winding about this geometry in length τ (1.94 mm) in the z direction.

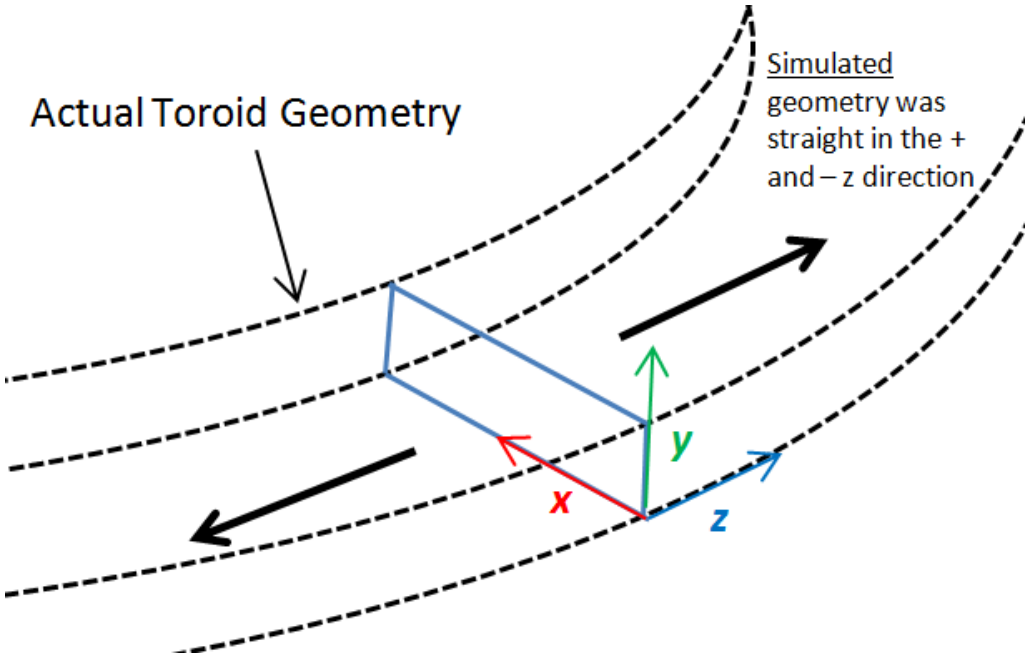

Figure 14: Coordinate system used in MATLAB code to simulate magnetic fields from wire winding current elements.

To solve Biot-Savart's Law, MATLAB code in Appendix B was used. An equal number of unit cells of wire were added onto each end of the central unit cell where the toroid unit cell domain exists. In the figures shown in this paper, 10 unit cells of wire were repeated on each end for a total of 21 unit cells. This wire was further broken down into straight, discrete elements of line current. For each plotted point in the toroid domain, the magnetic field created by each current element was summed together to get the final **H** field vector. Finally, the magnitude of the **H** field at each point in the toroid domain was calculated. Plots of magnetic field strength at various points in y on the x-z plane were made. Some of these plots are shown in Figures 15 through 17.

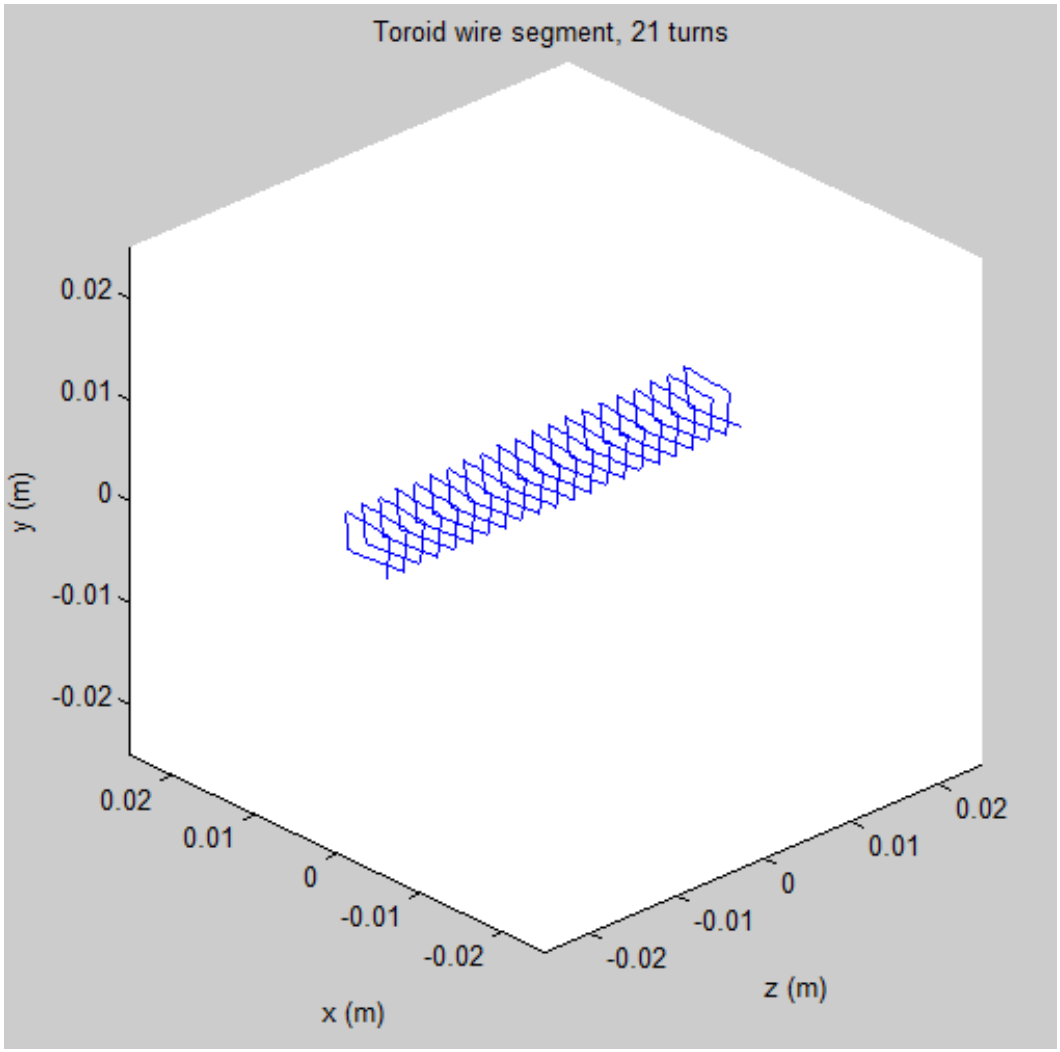

Figure 15: Line Currents Used to Estimate Magnetic Field. The coil consists 21 unit cells, or turns. Only the magnetic field produced within the very center of the coil, the center most unit cell, was calculated.

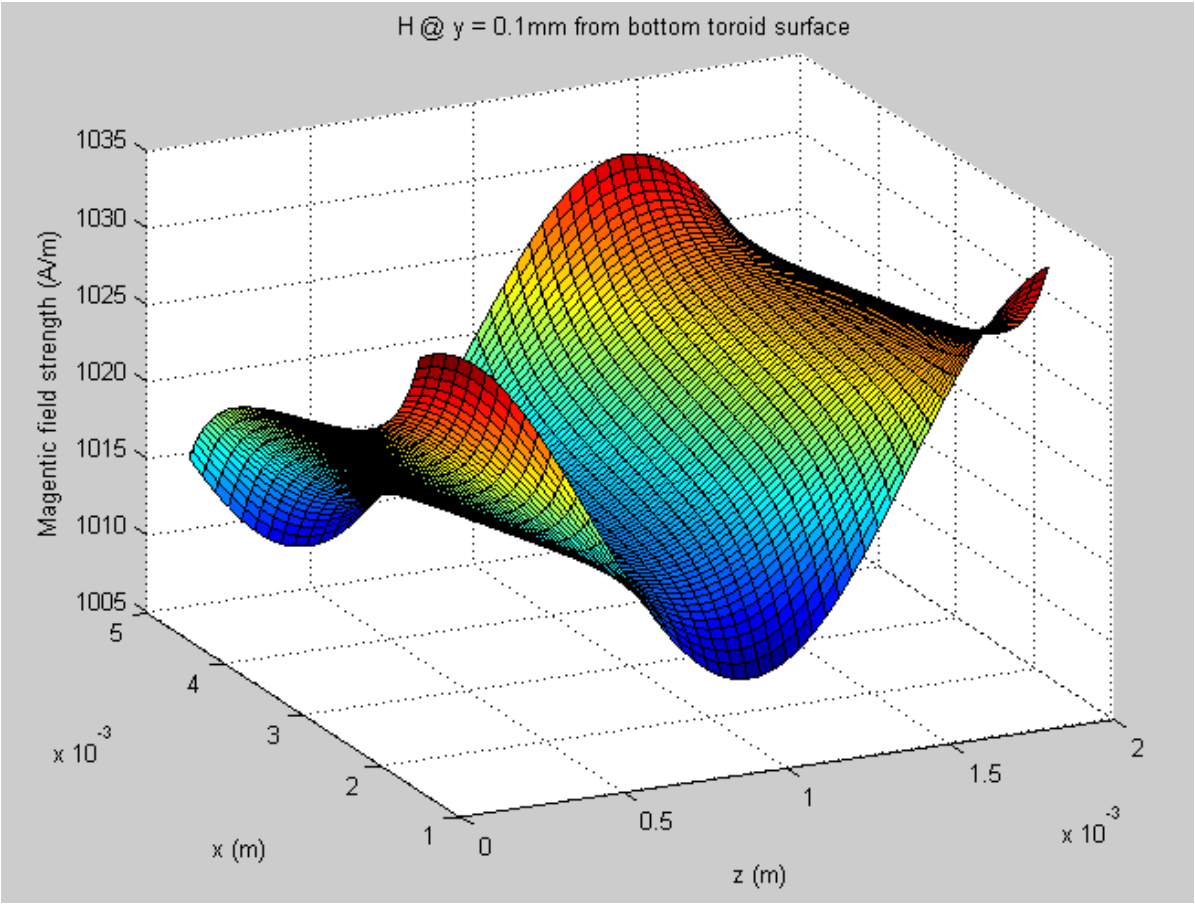

Figure 16: Calculated magnetic field strength near the bottom of the laminate stack (y = 0.1 mm) with current on wire equal to 2 A.

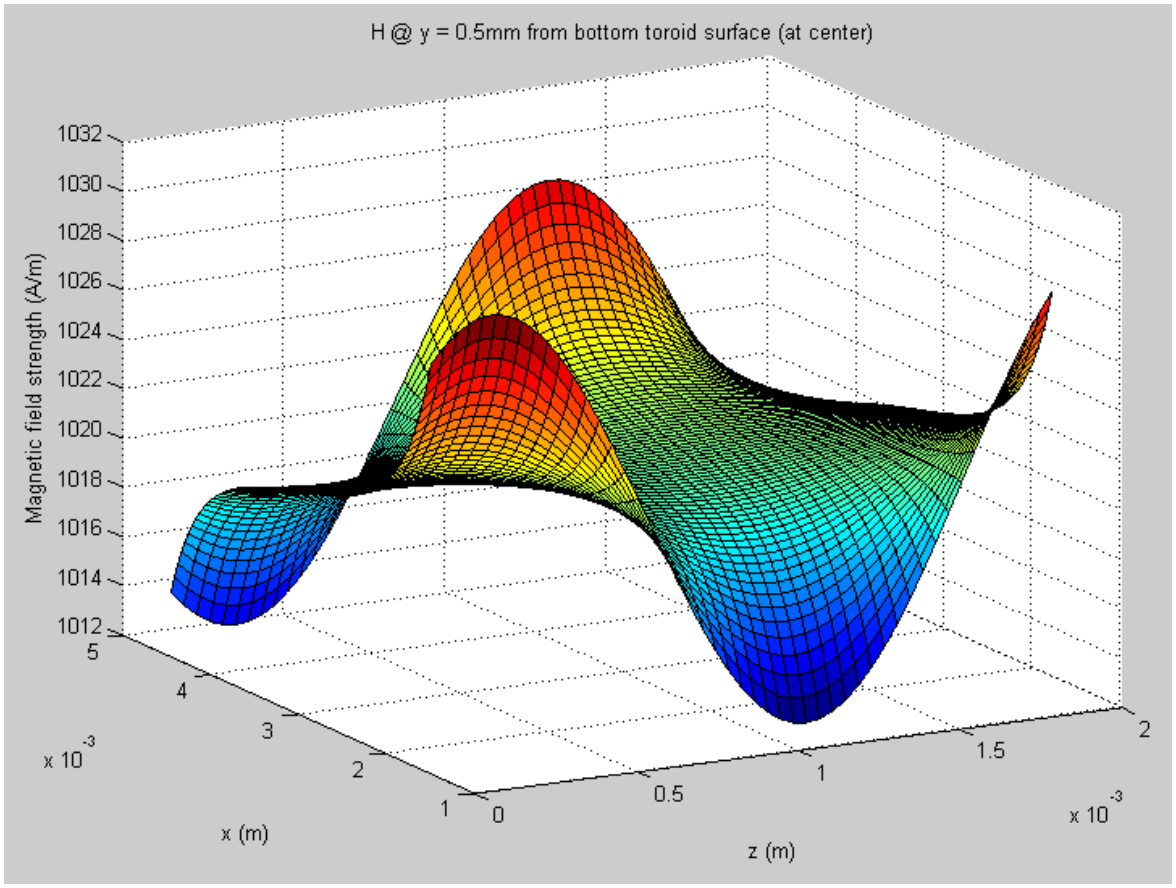

Figure 17: Calculated magnetic field strength near the center of the laminate stack (y = 0.5 mm) with current on wire equal to 2 A.

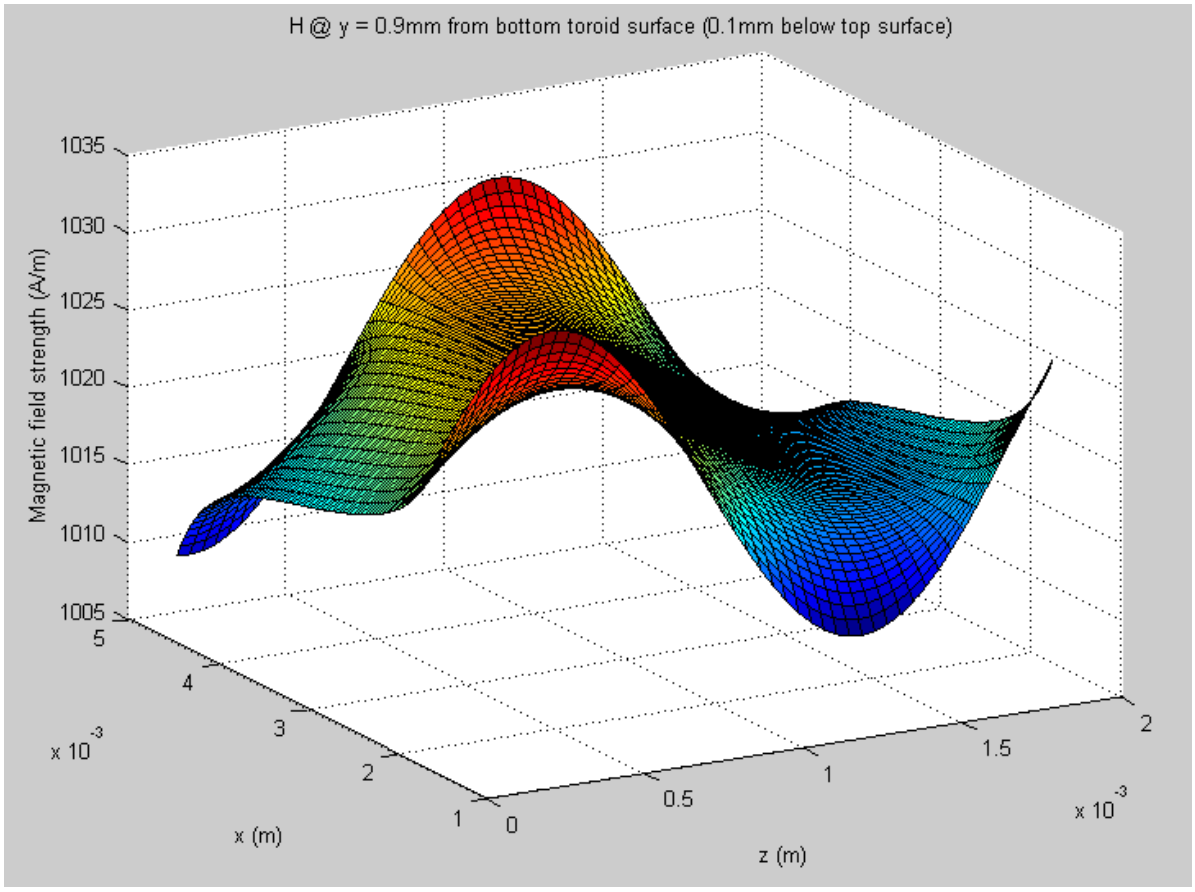

Figure 18: Calculated magnetic field strength near the top of the laminate stack (y = 0.9 mm) with current on wire equal to 2 A.

As can be seen in figures 16-18, the predicted magnetic field variation due to the wires is on the order of a few tenths of a percent. Thus, it is safe to conclude that the current distribution can be approximated as a uniform sheet current.

3.4.2 Variation in Magnetic Field Due to Cylindrical Spreading

Using the approximation that the current through the winding is effectively and accurately represented by a sheet current, the variation in magnetic field with respect to

radius due to cylindrical spreading can be established. To satisfy current conservation in cylindrical coordinates, the magnitude of the sheet current is given by:

$$|J_s| = \frac{NI}{2\pi r} = \frac{I_{tot}}{2\pi r} \tag{23}$$

where J_s is the sheet current (A/m), and I_{tot} is the total integrated current. Defining the sheet current on the inside surface of the toroid to be in the positive z direction, then the sheet currents for the four surfaces are:

$$\overrightarrow{J_s} = \begin{cases} \frac{I_{tot}}{2\pi a}\hat{z} \ \ on\ the\ inside\ surface \\ \frac{I_{tot}}{2\pi r}\hat{r} \ \ on\ the\ top\ surface \\ -\frac{I_{tot}}{2\pi b}\hat{z} \ \ on\ the\ outside\ surface \\ -\frac{I_{tot}}{2\pi r}\hat{r} \ \ on\ the\ bottom\ surface \end{cases} \tag{24}$$

Applying the definition of Ampere's Circuital Law given in equation 20, it is clear that I_{inc} is constant between $r = a$ and $r = b$, and is equal to NI. Thus, the exact solution to equation 20 for a sheet current can be found as follows.

Choosing the integration path to be $\overrightarrow{dL} = d\varphi\hat{\varphi}$, at a constant r within the range $a < r < b$, Ampere's Circuital Law becomes:

$$\int_0^{2\pi} \vec{H} \cdot r d\varphi\hat{\varphi} = I_{tot} \tag{25}$$

Solving this, one obtains:

$$2\pi r H_\varphi = I_{tot} \tag{26}$$

which can be rearranged into:

$$H_\varphi = \frac{I_{tot}}{2\pi r} \tag{27}$$

Note that in the case of a uniform sheet current, $H_\varphi \hat{\varphi} = \vec{H}$.

So due to equation 27, the magnetic field is expected to be strongest on the inside edge of the toroid and weakest on the outside edge. The variation in magnetic field with respect to r relative to the average radius r_o simplifies to:

$$\frac{r_o - r}{r_o} = \Delta H \qquad (28)$$

Values for ΔH are given in Table 3 below.

Variation in magnetic field with respect to r relative to the average radius r_o (ΔH)			
Toroid Name	#00028	#00042	#00058
ΔH, % relative to r_o	+8.00% inside edge, (r = a) -8.00% outside edge (r = b)	+8.11% inside edge, (r = a) -8.11% outside edge (r = b)	+8.11% inside edge, (r = a) -8.11% outside edge (r = b)

Table 3: Variation in Magnetic Field with Respect to Radius Due to Cylindrical Spreading.

3.4.3 Eddy Current Fields

The changing **B** field induces an electric field within the toroid according to Faraday's Law. In a material with a conductivity (σ) greater than 0, the induced electric field results in non-zero current density. These induced currents are known as "eddy currents", and they generate magnetic fields that oppose changes in flux. As a result, eddy currents reduce the effective applied magnetic field under AC excitation, especially towards the center of the sample where the sum of the magnetic fields produced by the eddy currents in opposition to the changing applied field is the greatest.

To determine whether the eddy current effects will be strong enough to affect the assumptions of uniform magnetic field in the sample, a theoretical approach is first taken to estimate the strength of the induced magnetic field by the eddy currents.

To understand the effects of eddy currents, start with differential form of Faraday's Law:

$$\nabla \times \vec{E} = -\frac{\partial \vec{B}}{\partial t} \tag{29}$$

In cylindrical coordinates, this becomes:

$$\left(\frac{1}{r}\frac{\partial E_z}{\partial \varphi} - \frac{\partial E_\varphi}{\partial z}\right)\hat{r} + \left(\frac{\partial E_r}{\partial z} - \frac{\partial E_z}{\partial r}\right)\hat{\varphi} + \frac{1}{r}\left(\frac{\partial (rE_\varphi)}{\partial r} - \frac{\partial E_r}{\partial \varphi}\right)\hat{z} = -\frac{\partial \vec{B}}{\partial t} \tag{30}$$

Due to the axial symmetry of $\vec{B}$ about the z axis, then $\frac{\partial \vec{E}}{\partial \varphi}$ must be zero, resulting in $\frac{\partial E_z}{\partial \varphi} = 0$ and $\frac{\partial E_r}{\partial \varphi} = 0$. Since $\vec{B}$ points only in $\hat{\varphi}$, then E_φ must be zero to make the $\hat{r}$ and $\hat{z}$ components of $\nabla \times \vec{E}$ equal to zero. Equation 30 simplifies to:

$$\left(\frac{\partial E_r}{\partial z} - \frac{\partial E_z}{\partial r}\right)\hat{\varphi} = -\frac{\partial B_\varphi}{\partial t}\hat{\varphi} \tag{31}$$

To estimate the value of the eddy current field effects, re-write Faraday's Law in integral form:

$$\oint \vec{E} \cdot \overrightarrow{dL} = -\frac{\partial}{\partial t}\iint_S \vec{B} \cdot \overrightarrow{dS} \tag{32}$$

In a material with conductivity (σ), the induced electric field from a changing flux results in non-zero current density according to Ohm's Law:

$$\vec{J} = \sigma \vec{E} \tag{33}$$

where $\vec{J}$ is the induced current density. Figure 19 is used to illustrate how these eddy currents reduce the effective applied **H** field towards the center of a lamination.

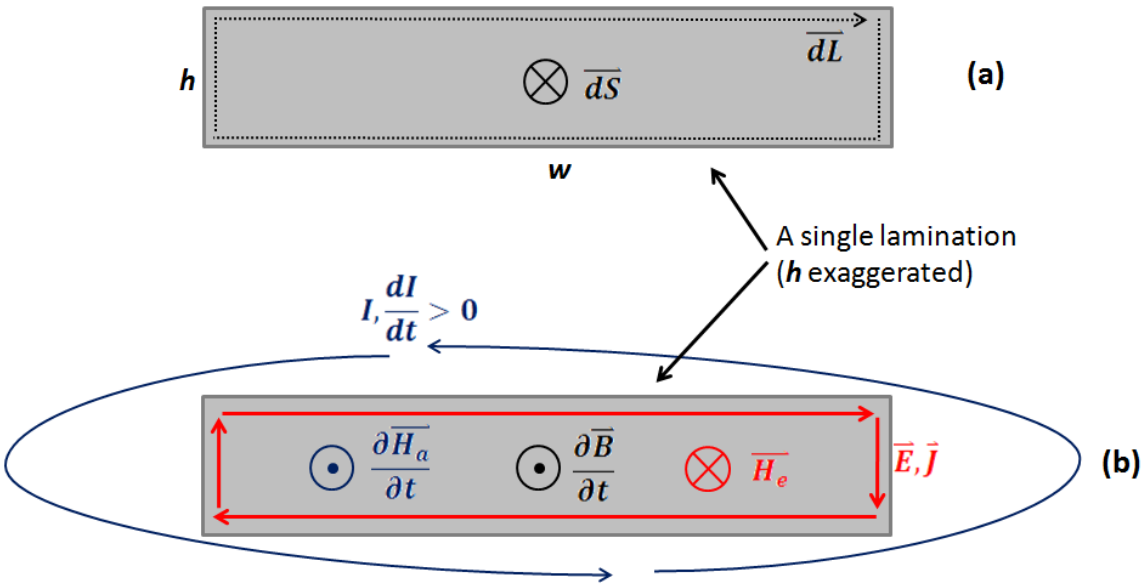

Figure 19 Eddy current schematic (a): Physical dimensions and vector differential elements for a single lamination and (b): Applied and induced fields

In Figure 19 (b), applied currents and fields are I and $\overrightarrow{H_a}$, and induced eddy currents and the fields created by them are given by $\vec{E}$, $\vec{J}$, and $\overrightarrow{H_e}$. The sum of the applied and induced fields creates the magnetic flux density $\vec{B}$:

$$\mu\left(\overrightarrow{H_a} + \overrightarrow{H_e}\right) = \vec{B} \tag{34}$$

where μ is defined as:

$$\mu = \mu_0 \mu_r \tag{35}$$

It is important to remember that as given by equations 32 and 33, eddy currents will lag the exciting current by approximately 90 degrees when the conductivity is very low, but as the conductivity increases, the eddy currents must become 180 degrees out of phase in order to cancel out the excitation field.

It is convenient to start with the assumption that eddy current effects will be minimal, and include four additional assumptions:

1) The electric field is parallel to the surface of the lamination.
2) The electric field is uniform along a dimension.
3) The contribution of the electric field along the h dimension (height) to the $\oint \vec{E} \cdot \overrightarrow{dL}$ integral is negligible.
4) The flux density throughout the lamination is uniform.

Assumption 1 follows from Ohm's law: the **E** field must point in the same direction as current flow, and the current most flow parallel to the surface as it cannot flow into or out of the surface. The electrical field, at least near the surface, must be parallel to it. Assumption 2 follows from Ohm's law and current conservation. Assumption 3 is due to the fact that $^{w}/_{h}$ (width over height of each lamination) is approximately 20, and that the electric field strength in the height dimension should be similar to the strength in the width dimension. For obtaining a rough estimation of eddy current and field strength, the two components of electric field along the height dimension can be ignored. Assumption 4 holds true for negligible values of induced eddy current fields. If assumption 4 fails, then a more detailed analysis of eddy current strength is needed, preferably with finite element analysis software.

Using the above assumptions and equations to evaluate the magnitude of the induced eddy current field, the value of $\vec{E}$ is first calculated. Since the direction the magnetic field vector is known, and using the assumption that the flux density will be uniform and perpendicular to the direction to the surface enclosed by $\overrightarrow{dL}$, it is determined that:

$$\left|\oint \vec{E} \cdot \overrightarrow{dL}\right| = \frac{\partial}{\partial t} B w_s h_s \tag{36}$$

where $\overrightarrow{dL}$ is a rectangular path through the lamination cross-section of height h_s and width w_s, where $h_s \leq h$ and $w_s \leq w$. This integration path is shown in Figure 20.

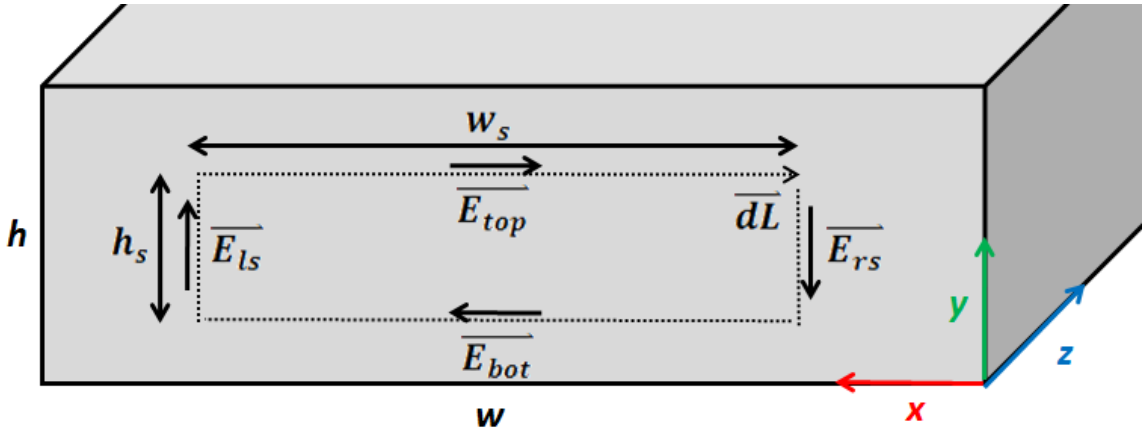

Figure 20: Schematic of an integration path for lamination cross-section.

Due to assumption 2 (i.e., the electric field is uniform along a dimension of the lamination), then $\overrightarrow{E_{top}} = \overrightarrow{E_{bot}}$, and $\overrightarrow{E_{ls}} = \overrightarrow{E_{rs}}$. Due to assumption 1 (i.e., that the electric fields are parallel to the surface), it can also be assumed that $\overrightarrow{E_{bot}} \cdot \hat{y} = \overrightarrow{E_{bot}} \cdot \hat{z} = 0$. Finally, assumption 3 gives the contribution of the electric field along the h dimension (height) to the $\oint \vec{E} \cdot \overrightarrow{dL}$ integral as negligible due to the aspect ratio of the lamination width versus the height. So the magnitude of $\oint \vec{E} \cdot \overrightarrow{dL}$ becomes:

$$\left|\oint \vec{E} \cdot \overrightarrow{dL}\right| = \left|\vec{E}\right| \int_0^{w_s} dx - \left|\vec{E}\right| \int_{w_s}^{0} dx \qquad (37)$$

$$\cong 2w_s E_x$$

where $\vec{E}$ is roughly uniform around L and points in the same direction as $\overrightarrow{dL}$, so that the values of E_y and E_z are zero.

Combining equation 37 with equation 36, the electric field becomes:

$$E_x \cong \frac{h_s}{2}\frac{\partial B}{\partial t} \qquad (38)$$

The eddy current density can be found using Ohm's law (equation 33):

$$\left|\vec{J}\right| = \sigma\left|\vec{E}\right| \cong \sigma\frac{h_s}{2}\frac{\partial}{\partial t}B \qquad (39)$$

To calculate the peak magnetic field produced by this eddy current distribution, a coordinate change to cylindrical is useful. The toroid center axis becomes the z axis and the rotation about the z axis becomes the φ axis. Next, h_s is replaced with $2z$ (as in this geometry, $h_s = 2z$), and then integrated around the closed path from $\varphi = 0$ to $\varphi = 2\pi$, $z = 0$ to $z = 0.5h$ (with h being the lamination thickness) at $r = r_o$. This gives the maximum current enclosed by the closed path L as:

$$\oint_C \vec{H} \cdot \overrightarrow{dL} = I_{tot} = \int_{0,}^{h_s/2,} \int_{0}^{2\pi} \sigma z \frac{\partial B}{\partial t} dz r d\varphi \qquad (40)$$

$$I_{tot} = \pi r_o \sigma \frac{h^2}{4}\frac{\partial B}{\partial t} \qquad (41)$$

where I_{tot} is the total current enclosed by the path L.

To solve for $\oint_C \vec{H} \cdot \overrightarrow{dL}$ at the center of the toroid, current conservation allows the use of equation 27 from before:

$$\oint_C \vec{H} \cdot \overrightarrow{dL} = 2\pi r_o H_\varphi \tag{42}$$

Combining 41 and42, the magnetic field generated by the eddy current distribution at the toroid center should be:

$$\left|H_\varphi\right| \cong \sigma \frac{h^2}{8} \frac{\partial B}{\partial t} = H_e \tag{43}$$

where: $H_z = 0$ and $H_r = 0$.

To calculate whether this field is non-negligible, experimental data for the value of μ_r is used. Inspection of the dynamic hysteresis plots in Chapter 4 shows that for the #00028 toroid, $\mu_r \sim 6000$ at flux density values significantly below the "knee". A "worst case" for the data presented in this paper is a maximum applied magnetic field of around 900 A/m, at a frequency of 1000 Hz. At this magnitude and frequency, then:

$$\frac{\partial B}{\partial t} = \mu_r \mu_o \omega H_o \cong 40000\ Wb/m^2/s$$

Using the conductivity of the Hiperco 50 material used in toroid #00028 from Table 1, the eddy current field strength is:

$$H_e \cong 240\ A/m$$

This is field level obviously *not* negligible, and thus a more detailed study of the eddy current effects was undertaken with finite element analysis software.

3.4.3.1 COMSOL Multiphysics simulation of Field with Eddy Current Effects

For a more accurate calculation of the magnetic field reduction due to the induced eddy currents within a toroid lamination, a model was developed in COMSOL Multiphysics 3.3 to roughly simulate the #00028 toroid. Six rectangular domains representing laminations (measuring 0.00282 m by 0.00014 m each) were stacked with a 10μm gap between each layer. These domains were placed at a distance from the z axis so that the center of the domains coincided with the r_o dimension of toroid sample #00028. The rectangular domains are effectively the same dimensions as the flat, laminations of the actual toroid, given the model's use of axial symmetry about the z-axis.

To represent the current through the coil, an outer rectangular domain encompassing all the laminations was created. Sheet current boundry conditions of the form expressed in equation 24 were applied to this domain's surfaces to represent the current through the coil. The value of I_{tot} (total value of all the sheet current combined) was set to 99.6 in order to achieve a nominal magnetic field of 900 A/m in the toroid's center. Finally, the values of conductivity within each of the six domains representing the laminations was set to the value of conductivity for Hiperco 50 material, and a relative permeability μ_r of 6000 (obtained from experimental results in Chapter 4) was used.

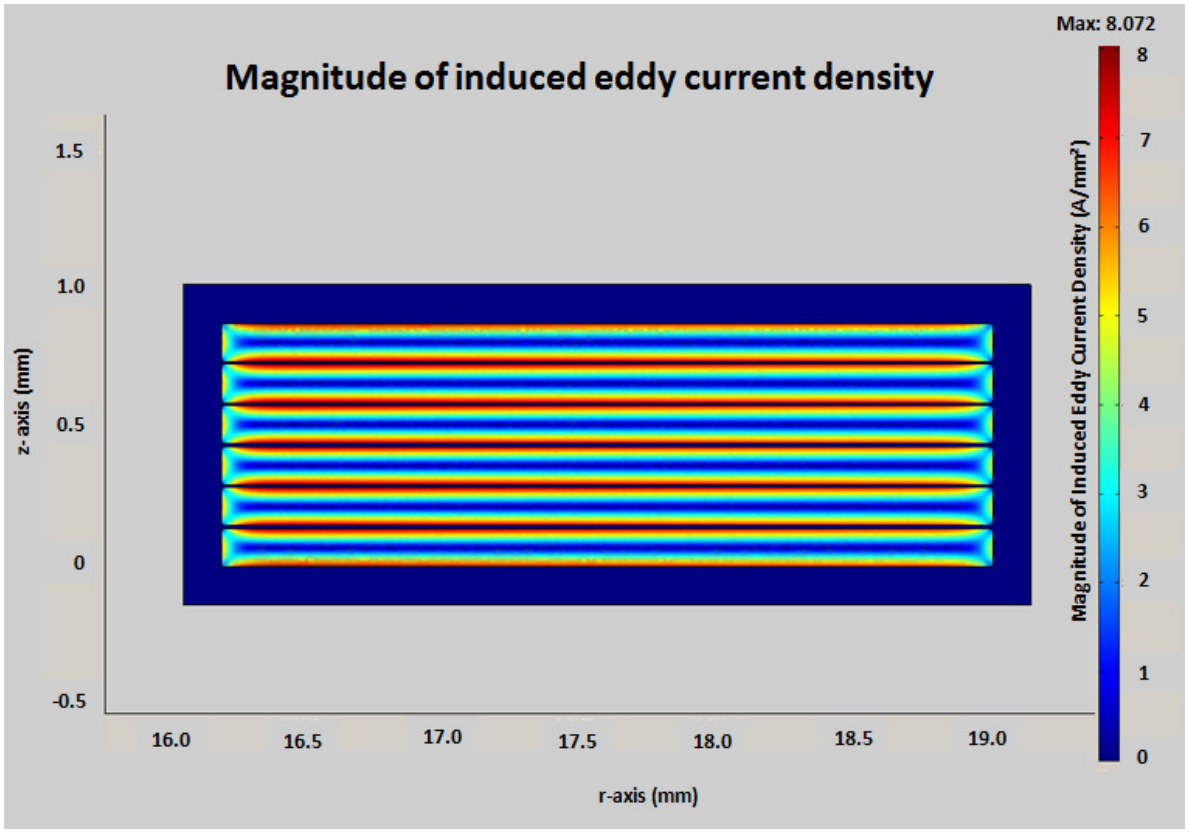

Figure 21: Simulation of induced eddy current density at 1000 Hz for representative #00028 toroid

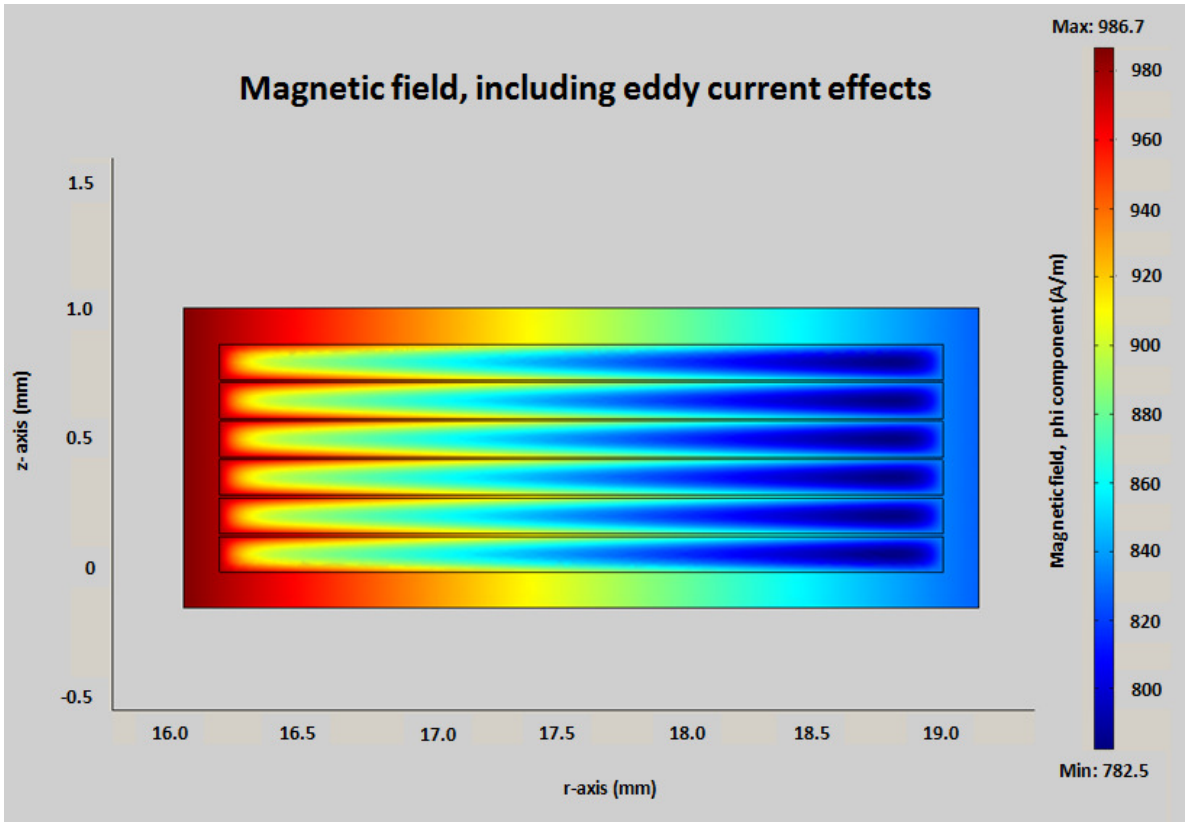

Figure 22: Simulation of Peak Magnetic Field at 1000 Hz for #00028 Toroid

Figure 22 displays a graphical representation of the spatial variation in magnetic field. The simulation demonstrates that the peak **H** field is reduced significantly by the induced eddy current field, by about 70 A/m.

It is worth noting that the simulation assumes a linear relationship between **B** and **H**, where in actuality, the relationship is highly non-linear at this high of a magnetic field level. Although this COMSOL simulation is only semi-quantitative, it corroborates the calculations from the previous section.

Additionally, note that as the eddy current induced fields are out of phase with the exciting field, the 70 A/m reduction predicted by COMSOL is not the magnitude of the induced fields themselves, but simply how much the peak field is reduced.

Chapter 4: Experimental Data and Analysis of Current and Voltage Sinusoids

4.1 Important Concepts and Results

This chapter presents differences in magnetic behavior of the three sample toroids. The primary focus is differences in core loss between sinusoidal current source and sinusoidal voltage source waveforms.

The relationship between voltage and current flowing through a typical coil will be largely inductive with a slight resistance representing the coil Ohmic losses, given by:

$$V_w = L\frac{dI}{dt} + IR_w \tag{44}$$

where V_w is the voltage on the winding, R_w is the winding resistance, and L is the inductance. It is important to remember that L is a function of μ_d:

$$L \cong \frac{\mu_d A N^2}{\ell_m} \tag{45}$$

where μ_d is the differential permeability, defined as:

$$\mu_d = \frac{dB}{dH} \tag{46}$$

and where ℓ_m is the mean magnetic path (in this case, $2\pi r_o$). For large signals, $\mu_d$will vary substantially and the magnetic system is highly non-linear. Because μ_d changes its value based on the total flux density contributed by all signals, the superposition principle fails. Analysis in the frequency domain becomes less useful for magnetic systems excited by high fields. [4]

When μ_d is linear, an applied sinusoidal current results in a sinusoidal voltage and vice-versa. When μ_d is nonlinear, a sinusoidal current (or voltage) will not result in a

sinusoidal voltage (or current). This suggests that differences in core losses between voltage source excitation and current source excitation of a coil should exist. A survey of published literature did not find a direct analysis and measurement of this difference for sinusoids. The results shown here are believed to be the first assessment of this kind.

Test standards often do not differentiate between voltage source and current source excitation. For example, IEEE Std 393-1991 *Standard Test Procedures for Magnetic Cores*, section 6.4 "Core-Loss Measurements With Sinusoidal/Voltage Excitation" does not clearly state whether a sinusoidal voltage or current is to be used to excite the core, though the statement that "the power source should have a low impedance" [5] seems to imply a sinusoidal voltage excitation is used as an ideal current source has infinite impedance.

To explore these differences, toroids #00028, #00042, and #00058 were subjected to 1 kHz sinusoidally varying current or voltage waveforms using the hysteresisgraph system described in Chapter 2. The voltage across the secondary winding was recorded and analyzed as described in Chapter 2.2 and Chapter 3.3.

To capture and accurately characterize the normal magnetization curve, twenty datasets were made for each material under each excitation method, with datasets taken at maximum magnetic fields (**H**) of 25, 50, 75, 100, 125, 150, 175, 200, 233, 267, 300, 333, 367, 400, 450, 500, 600, 700, 800, and 900 A/m. Plots of current on the primary coil and voltage on the secondary coil against time are shown in figures 23 through 34.

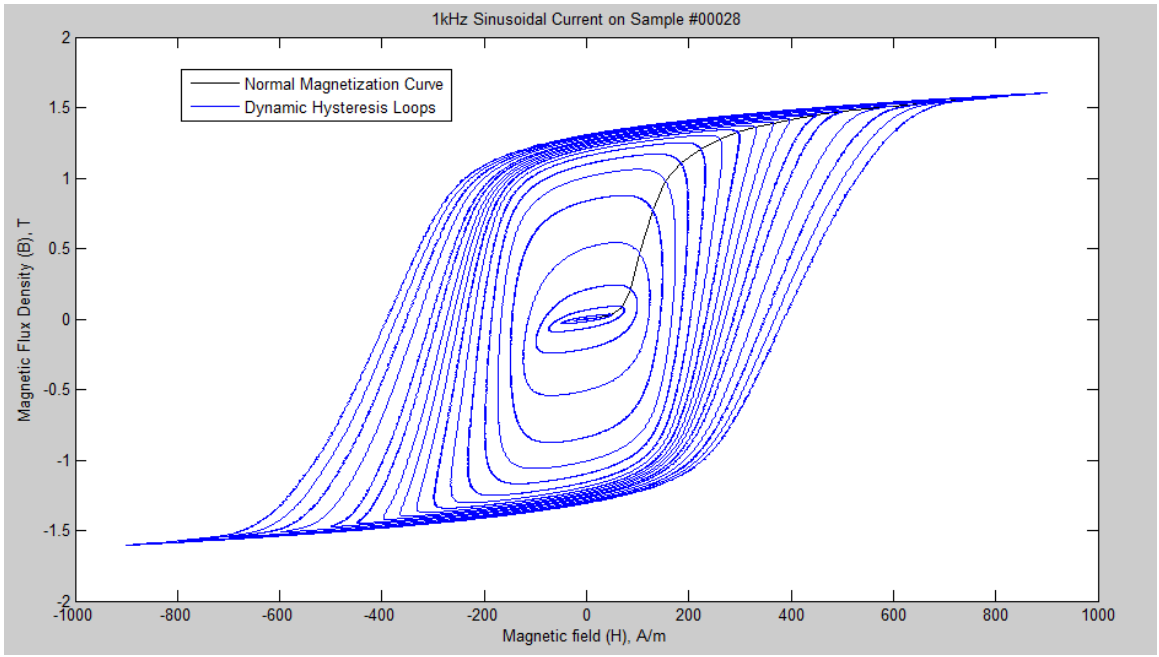

Figure 23: 1 kHz Sinusoidal Current Dynamic Hysteresis Loops for Toroid #00028

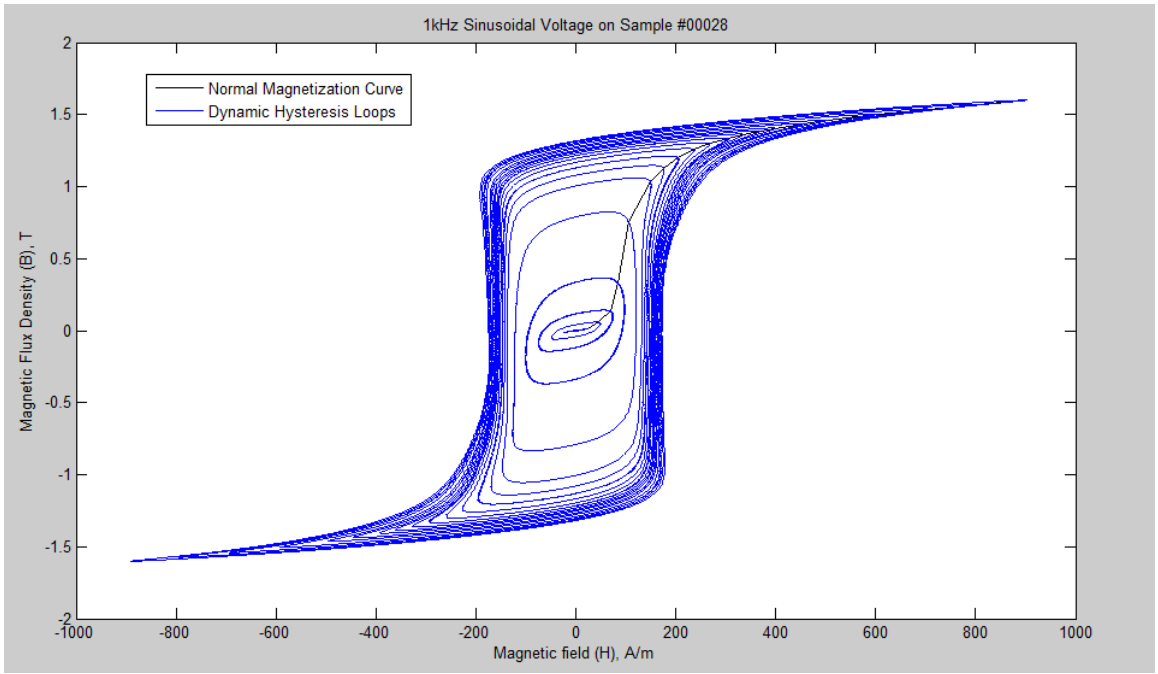

Figure 24: 1 kHz Sinusoidal Voltage Dynamic Hysteresis Loops for Toroid #00028

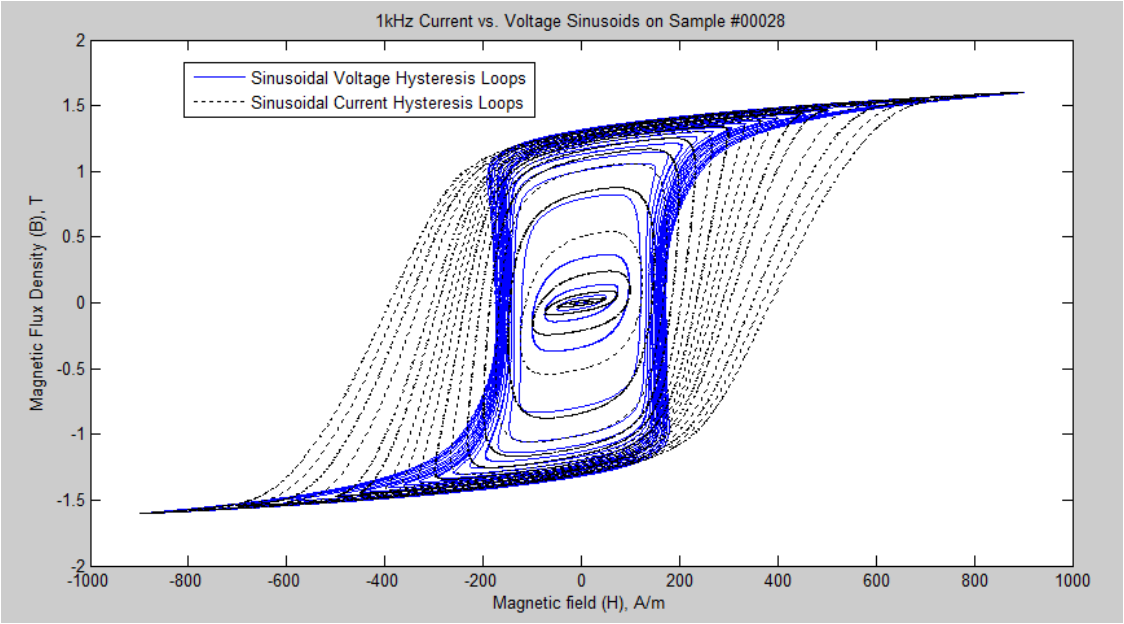

Figure 25: Comparison of Current and Voltage Sinusoid Dynamic Hysteresis Loops for Toroid #00028

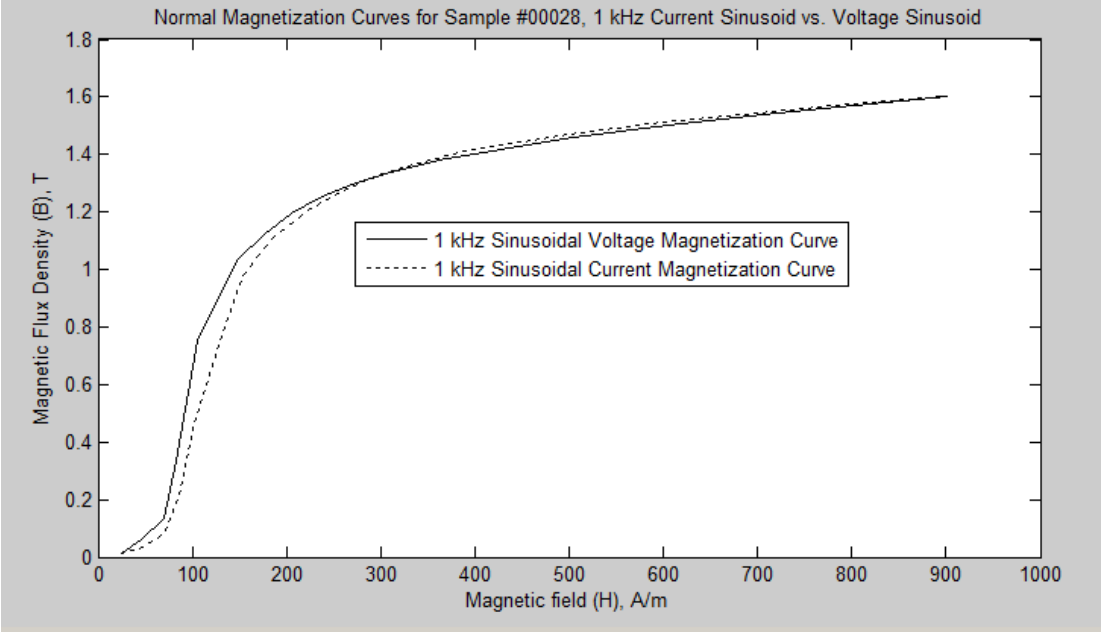

Figure 26: Comparison of Magnetization Curves of Toroid #00028 by Sinusoidal Current and Voltage Excitation

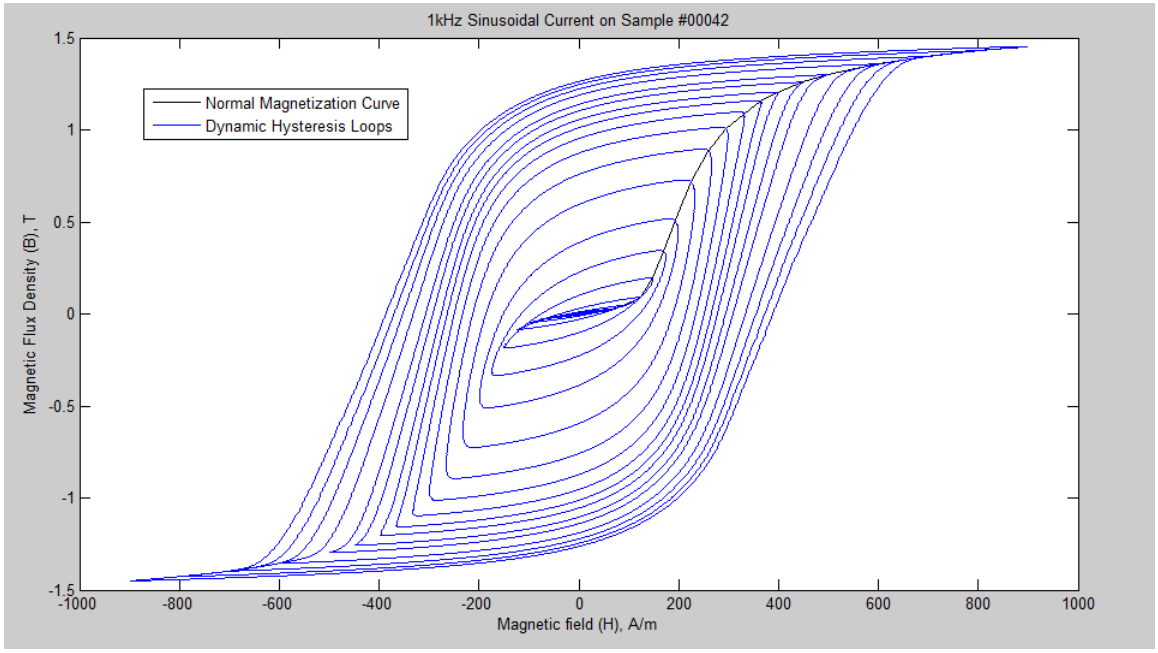

Figure 27: 1 kHz Sinusoidal Current Dynamic Hysteresis Loops for Toroid #00042

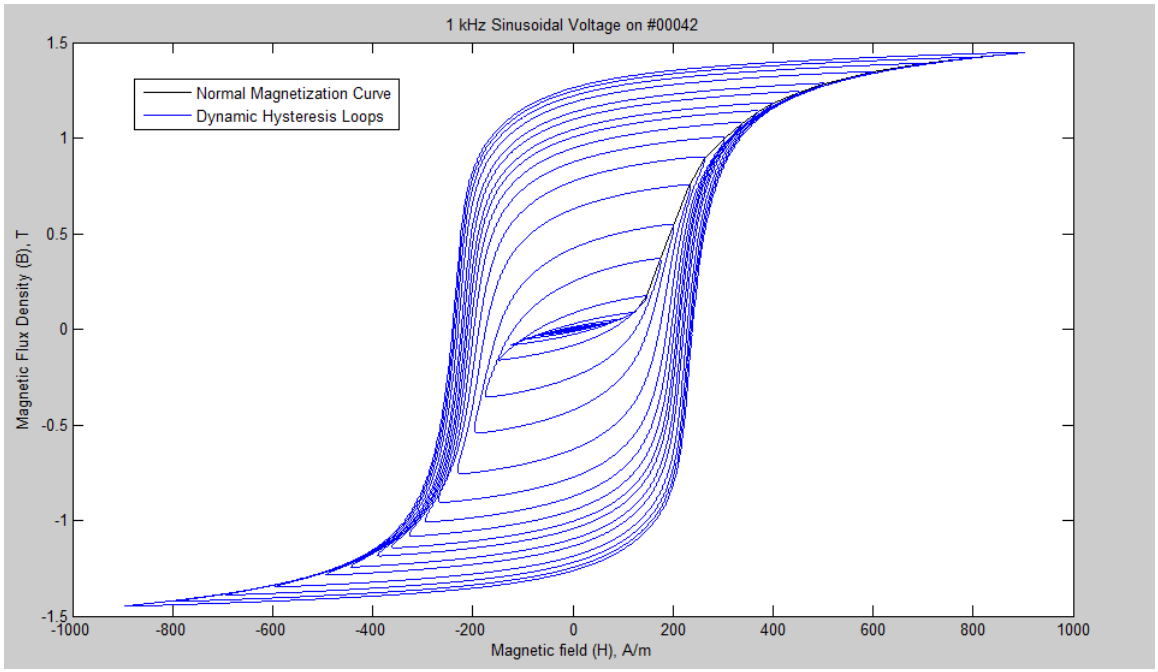

Figure 28: 1 kHz Sinusoidal Voltage Dynamic Hysteresis Loops for Toroid #00042

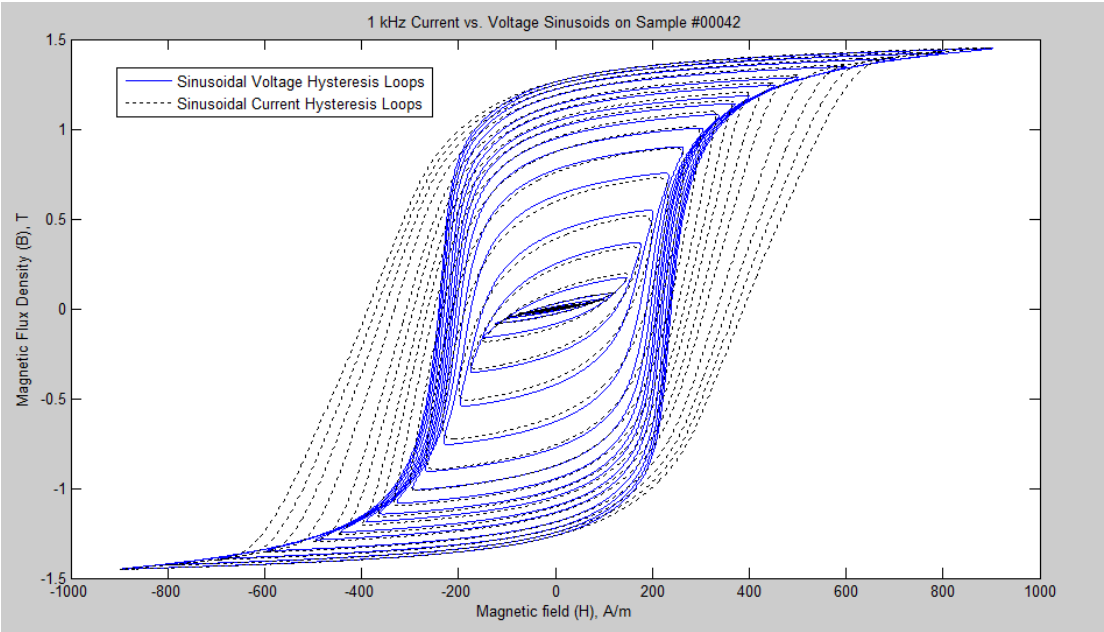

Figure 29: Comparison of Current and Voltage Sinusoid Dynamic Hysteresis Loops for Toroid #00042

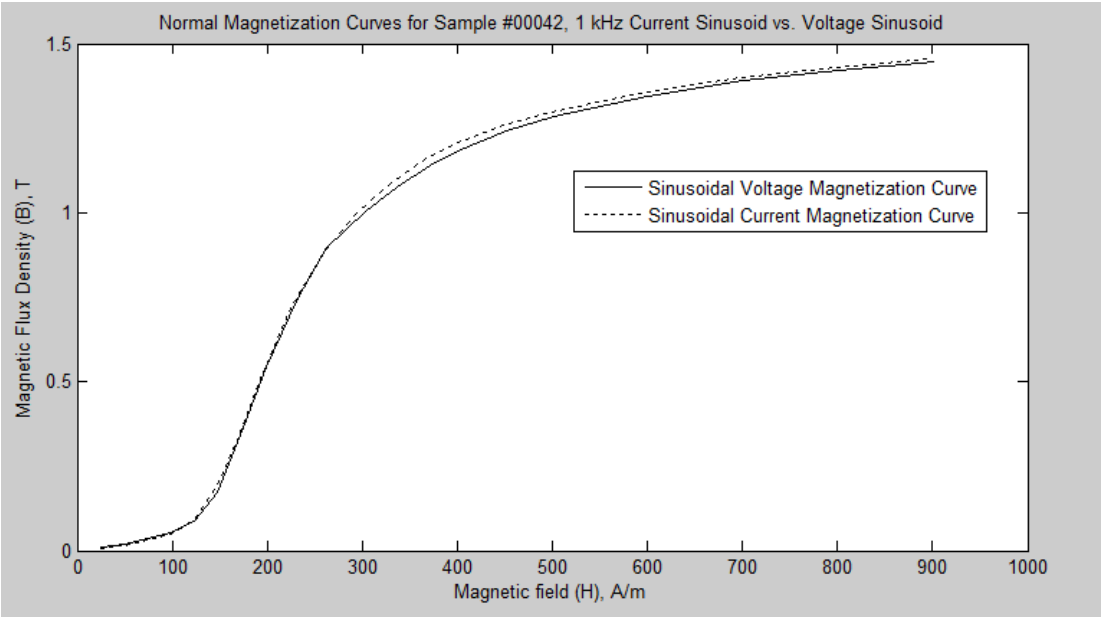

Figure 30: Comparison of Permeability of Toroid #00042 by Sinusoidal Current and Voltage Excitation

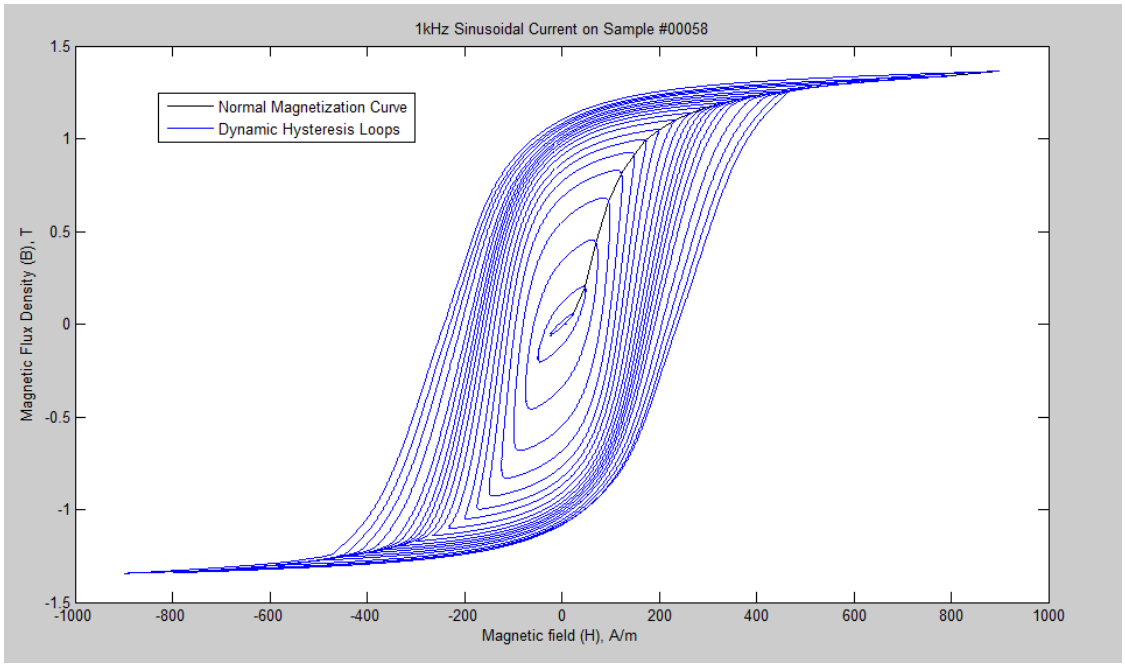

Figure 31: 1 kHz Sinusoidal Current Dynamic Hysteresis Loops for Toroid #00058

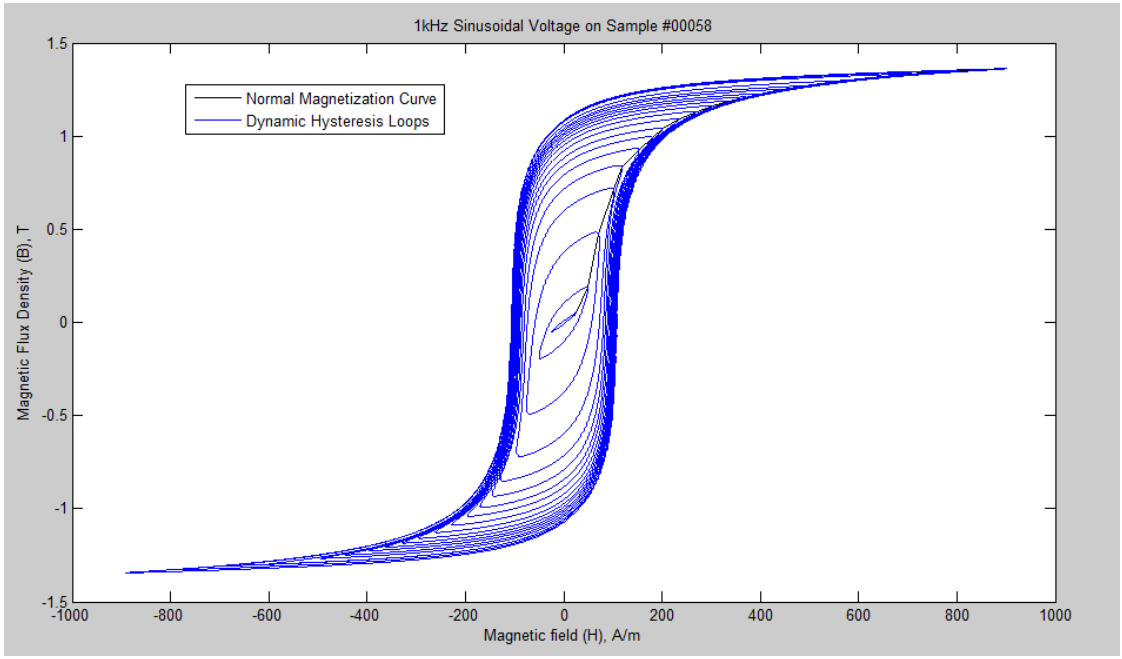

Figure 32: 1 kHz Sinusoidal Voltage on Toroid #00058

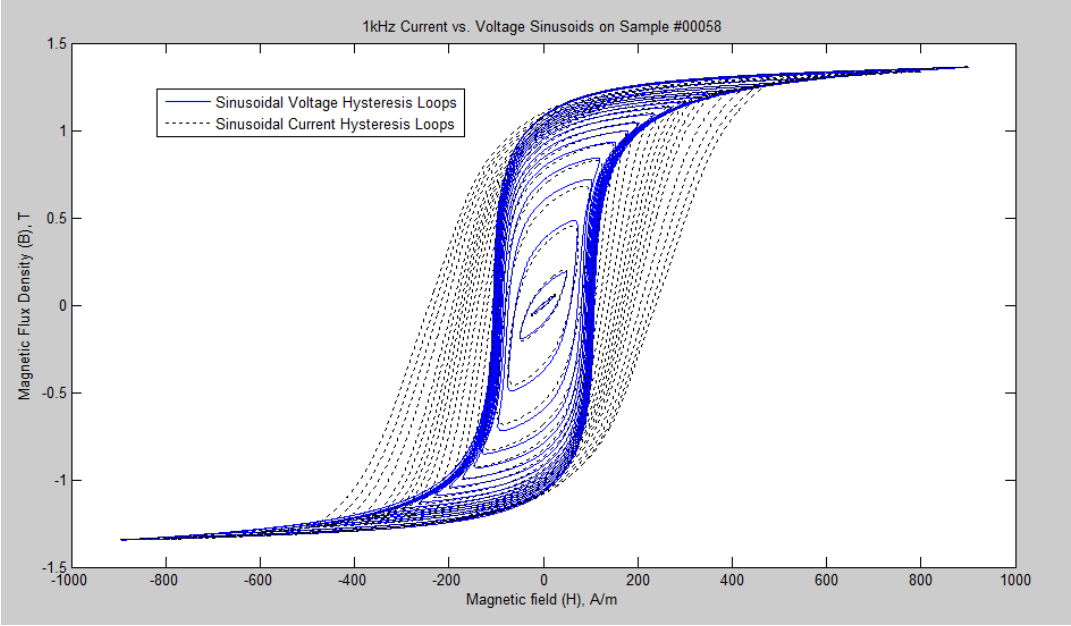

Figure 33: Comparison of Current and Voltage Sinusoid Hysteresis Loops for Toroid #00058

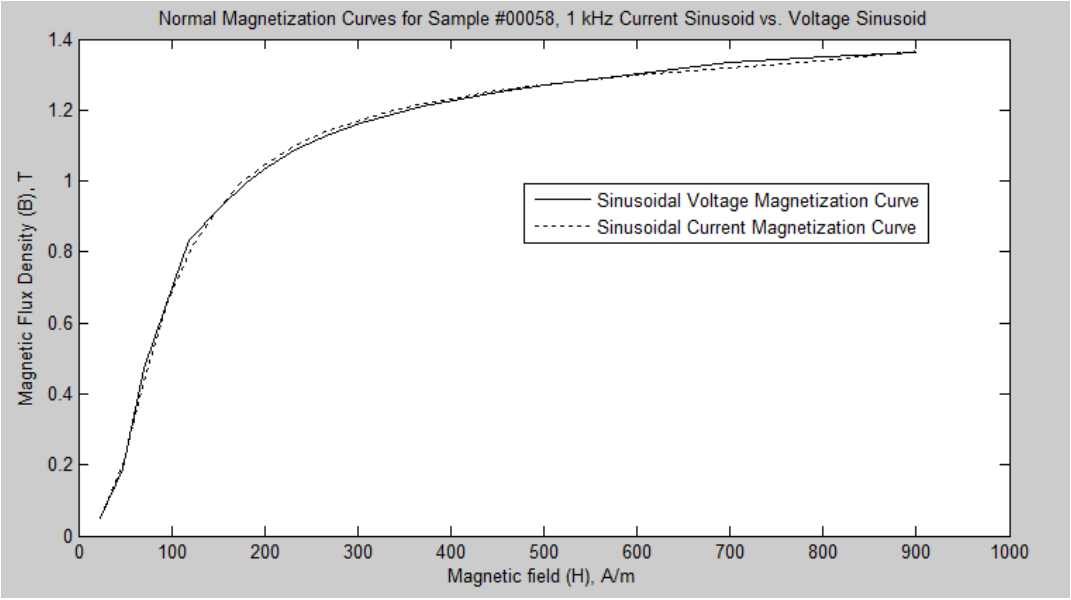

Figure 34: Comparison of Normal Magnetization Curves of Toroid #00058 by Sinusoidal Current and Voltage Excitation

When analyzing these datasets, particular interest was paid to the specific energy loss in a cycle, represented by the area inside a dynamic hysteresis loop. The normal magnetization curve was also examined. As the free space flux contribution was, for all materials, negligible compared to the magnetization of the material (so, $\mu_r \gg 1$), there was no need subtract it from the normal magnetization curves.

It is important to remember that the core loss per cycle is proportional to the area enclosed by a dynamic hysteresis loop on a **B**-**H** plot. This is because field energy is given by:

$$W_f = \int_0^{\lambda} id\lambda \tag{47}$$

where λ is the flux linkage $N\phi$, and i is the current applied to a coil with turns N. [6] Recalling that $B = {\phi}/{A}$ and $H = \frac{Ni}{l}$, then equation 47 in terms of **H** and **B** becomes:

$$W_f = \int_0^{NBA} \frac{lH}{N} dNB\,A = lA \int_0^{B} HdB \tag{48}$$

The specific energy stored, the energy stored per unit volume, is:

$$W_s = \int_0^{B} HdB \tag{49}$$

which is, graphically, the area between the B axis and the **B**-**H** curve.

On a graph of a hysteresis loop, this loss causes the **B**-**H** curve to trace a different path upon demagnetization. Core loss per cycle per unit volume is the graphical area on the **B**-**H** characteristic enclosed by a single dynamic hysteresis loop, expressed mathematically as the closed line integral of $\boldsymbol{H}d\boldsymbol{B}$:

$$L_s = \oint HdB \tag{50}$$

This approach is useful in visually estimating hysteresis loss, but when integrating its value from measured data (which usually exists as measurements of current through a primary coil,

voltage across a secondary coil, and time) it is easier to use equation 19 in Chapter 3.3:

$$W = \frac{1}{2\pi r_o A}\int_0^T i_1(t)\, v_2(t) dt \qquad (19)$$

Consider that when non-negligible eddy currents exist, the flux density **B** represented in figures 23 through 34 represents the spatial average flux density. Eddy currents near the surface of a toroid lamination will cause the magnetic field to decrease in magnitude near the center of the lamination, as was demonstrated in Chapter 3.4.3.

Test results demonstrated very clear and significant differences between sinusoidal current excitation and sinusoidal voltage excitation. In particular, sinusoidal current excitation consumes more electrical power and creates more core loss. This will be explained by the effects of eddy currents, as discussed later in Chapter 4.2. Additional results were found in some cases that seem to indicate that the sinusoidal voltage and current source excitations appear to have different normal magnetization curves. A possible explanation of this is also offered in Chapter 4.2.

To verify that the differences seen in the normal magnetization curves were real and not the result of plotting methods, two different methods were used to plot the normal magnetization curves. The first method was to plot the magnetization curves based on the points in the dynamic hysteresis loops where the measured values of **B** and **H** had the highest product. When the maximum **B** and maximum **H** values for a loop do not occur at the same point, this represents an intermediate point on the curve between them. This method was used for the normal magnetization curves shown in all plots. A second method tried was to plot the normal magnetization as a function of the intercepts between the maximum **B** and maximum **H** values for each dynamic hysteresis loop. Only slight differences were found between these two methods.

4.2 Discussion of Results

The hysteresis loops at 1 kHz tend to have higher losses when a sinusoidal current source waveform is used. This can be seen by the larger areas enclosed by their hysteresis loops in figures 25, 29, and 33. Excitation with 1 kHz voltage sinusoids produced consistently lower power loss for all three toroid samples.

4.2.1 Eddy Currents

The lower losses under sinusoidal voltage excitation can be most readily explained by examining the strength of the eddy current fields generated within the toroids in current source and voltage source excitation. Recalling Faraday's Law, the voltage on the secondary coil is:

$$V_{sw} = -N\frac{\partial \Phi}{\partial t} \tag{51}$$

and within the material of the toroid itself (assuming a uniform Φ distribution):

$$-\frac{1}{n_{lam}}\frac{\partial \Phi}{\partial t} = \oint \overrightarrow{E_c} \cdot \overrightarrow{dL_c} \tag{52}$$

where V_{sw} refers to the potential difference between the two ends of a secondary winding (carrying no current), $\overrightarrow{E_c}$ is the electric field in the core, L_c is the closed path through the perimeter of the cross-section of the lamination, Φ is the total flux, and n_{lam} is the number of laminations. The relationship between the electric field within a lamination and the voltage one the secondary coil is then:

$$\oint \overrightarrow{E_c} \cdot \overrightarrow{dL_c} = \frac{1}{N \cdot n_{lam}} V_{sw} \tag{53}$$

and recalling that,

$$\oint \vec{E} \cdot \overrightarrow{dL} = V \tag{54}$$

where V is a voltage, it is easy to see the relationship between the voltage on the coil and the magnitude of eddy currents is:

$$V_c = \frac{1}{N \cdot n_{lam}} V_{sw} \tag{55}$$

which means that:

$$V_{sw} \propto V_c \tag{56}$$

where V_{sw} is the voltage on the wire coil and V_c is induced EMF around the permimeter of the lamination/core. Squaring equation 56, the power lost in the core due to eddy currents is proportional to:

$$P_{eddy} \propto {V_{sw}}^2 \tag{57}$$

To help understand why the dynamic hysteresis loops excited by sinusoidal current and voltage sources differ so much, first consider the case of sinusoidal voltage field excitation where R_w in equation 44 is much less than $L\frac{dI}{dt}$. In this case, the voltage on the secondary winding can be expressed as:

$$V_{sw,v} \cong V_{pw,v} = V_o e^{j\omega t}, \quad (when\ L\frac{di}{dt} \gg iR_w) \tag{58}$$

where $V_{pw,v}$ is the sinusoidal voltage on the primary, $V_{sw,v}$ is the sinusoidal voltage on the secondary, and V_o is the peak voltage of the sinusoid. Also, consider the voltage on the secondary coil from a sinusoidal current excitation,

$$V_{sw,c} = L\frac{dI}{dt} = j\omega L I_o e^{j\omega t} \tag{59}$$

where I_o is the peak value of the current sinusoid. Replacing L with equation 45:

$$V_{sw,c} = L\frac{dI}{dt} = j\omega \frac{\mu_d A N^2}{\ell_m} I_o e^{j\omega t} \tag{60}$$

The differential permeability is nonlinear and very difficult to predict. [7] Assuming that a material is excited to the same maximum flux density with two different waveforms, then while the actual waveforms will be different, the integral over time of the voltage on the secondary winding for each waveform will be the same from $t = 0$ to $\frac{T}{2}$, where t is defined to be at the minimum or maximum flux and T is the period of voltage or current waveform:

$$\int_0^{T/2} V_{sw,c}\,dt = \int_0^{T/2} V_{sw,s}\,dt \tag{61}$$

$$\int_0^{T/2} j\omega \frac{\mu_d A N^2}{\ell_m} I_o e^{j\omega t}\,dt = \int_0^{T/2} V_o e^{j\omega t}\,dt \tag{62}$$

4.2.2 Eddy Currents and Loss

Since the voltage waveforms for two different signals must integrate to the same value in the same period of time, (to reach the same flux levels), that implies that the voltage on the

secondary coil for the current and voltage sinusoidal excitations must have the same average absolute value. However, since equation 57 indicates that eddy current loss is proportional to the voltage squared on the secondary coil, then a waveform with less "normalized mean square value" should result in less eddy current loss. The "normalized mean square" is defined by first normalizing the signal to its average value, and then taking the mean square of the result:

$$NMS\big(f(x)\big) = \frac{1}{T}\int_0^T \left(\frac{f(x)}{\frac{1}{T}\int_0^T |f(x)|dx}\right)^2 dx \qquad (63)$$

The signal with the least normalized mean square would be a square wave, so a square wave voltage appearing on secondary would in theory have the least eddy current loss for a signal of its average absolute value.

A sine wave, on the other hand, will have a higher mean square value after being normalized to its average value, as is shown below. For simplicity, this calculation uses the positive half of a period instead of the average absolute value:

$$NMS(\sin(x)) = \frac{1}{\pi}\int_0^\pi \left(\frac{\sin x}{\frac{1}{\pi}\int_0^\pi \sin x dx}\right)^2 dx = 1.23 \qquad (64)$$

While it's conceivable that a function of μ_d could result in a current sinusoid with significantly less eddy current loss than a voltage sinusoid (the current sinusoid would have to excite a voltage on the secondary that had a lower normalized mean square), it would not be common. However, it should be noted that harmonic effects and losses in motors typically mean that square waves will not reduce motor losses. [8], [9]

The dynamic hysteresis loops shown in figures 23 through 33 show that at peak flux values significantly below the knee of the curve, the hysteresis loops of the current and voltage sinusoids overlay fairly well for the #00042 and #00058 toroids. However, to reach the same peak *flux* in for the #00028 toroid, a current sinusoid has to have a significantly higher peak magnetic field (**H**) to achieve the same peak flux density. Inspection of Figure 25 suggests that, for example, if a peak flux density of ~0.8T is desired, then a 20% higher peak **H**-field excitation will be required of the current sinusoid as compared to the voltage sinusoid. One way to explain this is that, as previously mentioned, eddy currents will reduce the magnetic field in the center of a toroid lamination; if large eddy current effects are present, it will require more current to reach the same peak flux.

To explain what happens for hysteresis curves that pass far beyond the knee of the magnetization curve, then it is helpful to remember the toroid model as an inductor with nonlinear differential permeability. Substituting equation 45 into equation 44 one has:

$$V = \frac{\mu_d A N^2}{\ell_m}\frac{dI}{dt} + IR_w \qquad (65)$$

where μ_d is a nonlinear function of several different variables.

A universal property of $\mu_d$for magnetic materials is that at a high enough flux level, μ_d will begin to drop and approach its free-space value of $4\pi \times 10^{-7}$. Thus, the value of the voltage generated by the inductance across the coil, $V = L\frac{\partial I}{\partial t}$, should drop. This predicts a large voltage spike under strong sinusoidal current excitation as the current passes through zero, the magnitude of the spike determined mostly by $\frac{dI}{dt}$ and maximum magnitude of μ_d.

In comparison, for sinusoidal voltage excitation, the current peak would be expected somewhere between the voltage peak, and where the voltage passes through zero. Equation 65 shows why this is so: as μ_d decreases, the coil current eventually becomes limited by the impedance, not of the toroid inductance, but of the wire resistance, which is much smaller. This forces the current to peak at or after the voltage peak. This leads to another conclusion:

that the loss in the toroid due to eddy currents should, for flux densities approaching saturation, always be higher for current sinusoids than for voltage sinusoids. The sinusoidal current must reach its peak value of flux faster than the voltage sinusoid has to. Thus, the voltage peak must be higher in current excitation, and thus, the eddy current losses must be higher according to equation 57. Figure 35 demonstrates this graphically with collected data.

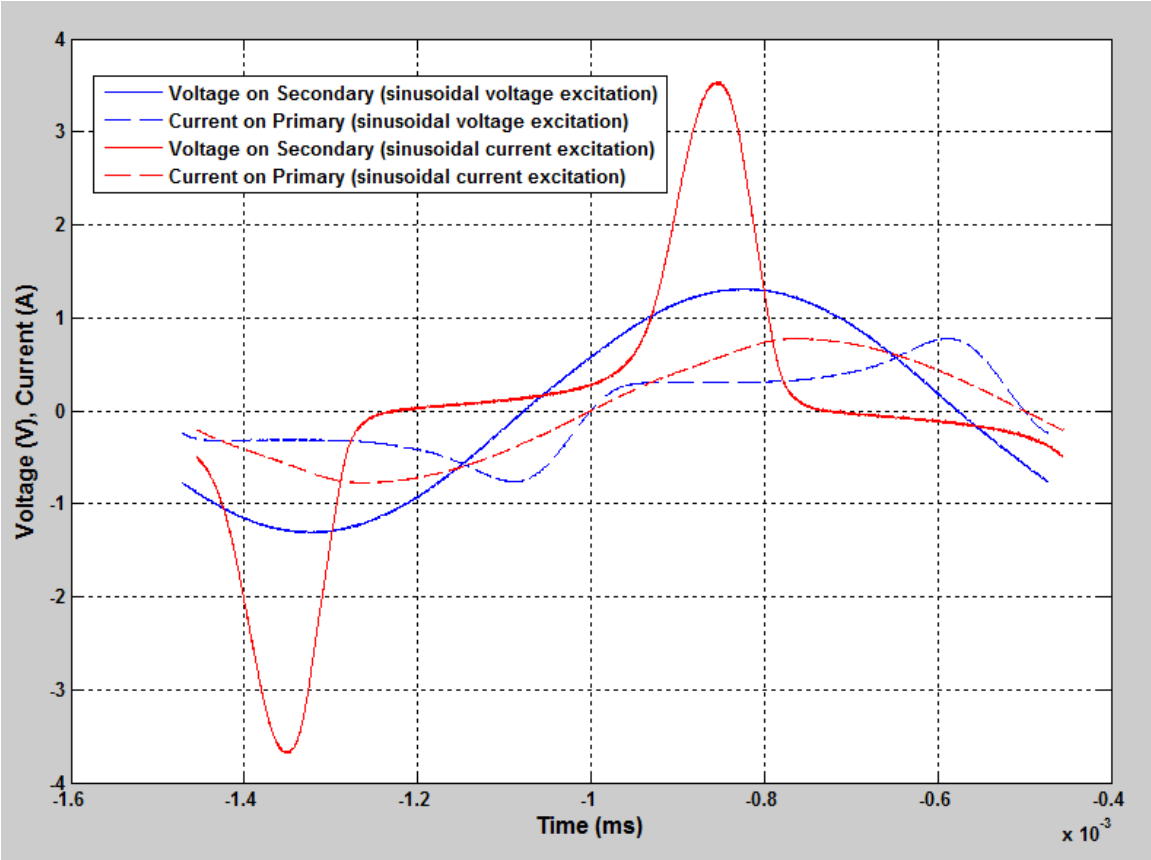

Figure 35: Comparison of Voltage and Current Waveforms of Sinusoidal Current Excitation and Sinusoidal Voltage Excitation at peak **H** of 400 A/m. This figure illustrates how the voltage waveform of the sinusoidal current is forced to peak much earlier and drop to zero as the material becomes effectively saturated. The voltage in sinusoidal current excitation peaks to a much higher value than the voltage in sinusoidal voltage excitation, causing more loss.

4.2.3 Differences in Magnetization Curves

Figures 26, 30, and 34 plot the normal magnetization curves of the three samples under the two excitation methods. The magnetization curves shown in Figures 30 and 34 for toroid samples #00042 and #00058, respectively, show little difference between sinusoidal current and voltage source excitation. However, the magnetization curve for toroid sample #00028, Figure 26, displays some interesting differences. The peak **B** times **H** product points do not follow the same curve for the two excitation methods. It is thought that this may be related to eddy current effects also, but if so, then such an effect should be strongest on sample #00042, which has the highest conductivity of the three samples. As the exact mechanism to explain this phenomenon is not yet clear, further study is required.

4.2.4 Comparison of Core Losses

For all dynamic hysteresis loops, the core loss was measured by using equation 19 in Chapter 3.3, integrated through MATLAB. While core loss can be seen graphically in figures 23 through 33 as the area enclosed by the dynamic hysteresis loop, it is useful to directly plot and compare it, as is done next. This data is presented in two different ways in figures 36 through 41: in figures 36, 38, and 40, specific loss is plotted against the magnitude of the exciting magnetic field. In figures 37, 39 and 41, specific loss is plotted against the max flux density, which is more physically relevant to machine operation.

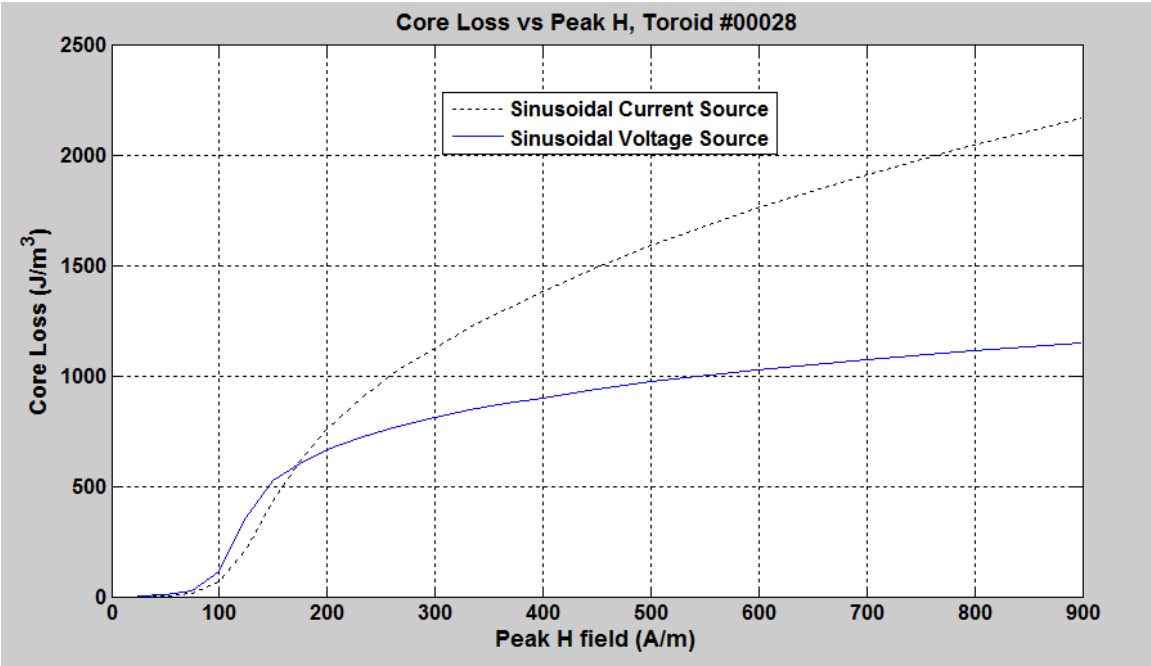

Figure 36: Core Loss (per cycle) vs. Peak Applied **H** Field, Toroid #00028

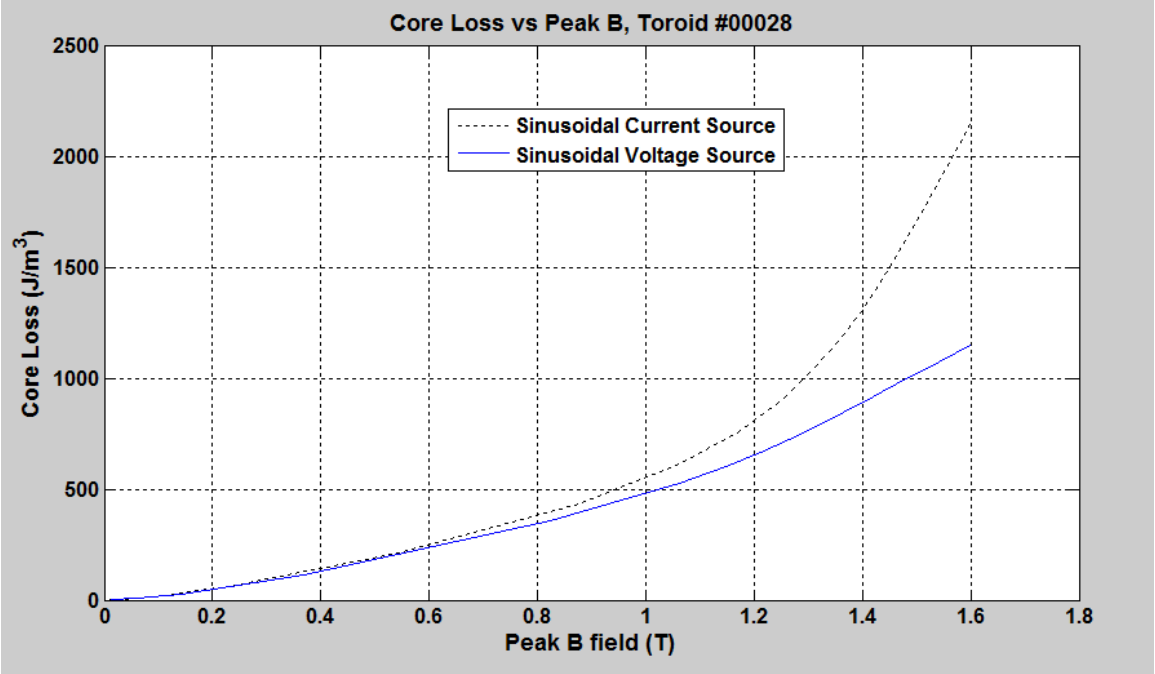

Figure 37: Core Loss (per cycle) vs. Peak Applied **B** Field, Toroid #00028

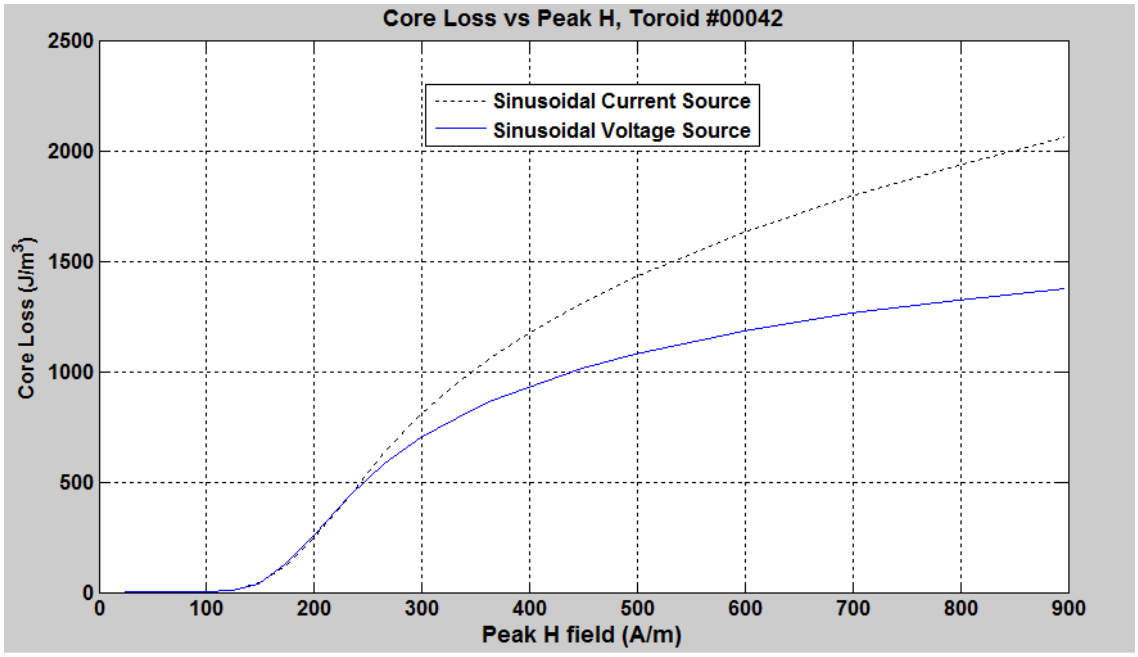

Figure 38: Core Loss (per cycle) vs. Peak Applied **H** Field, Toroid #00042

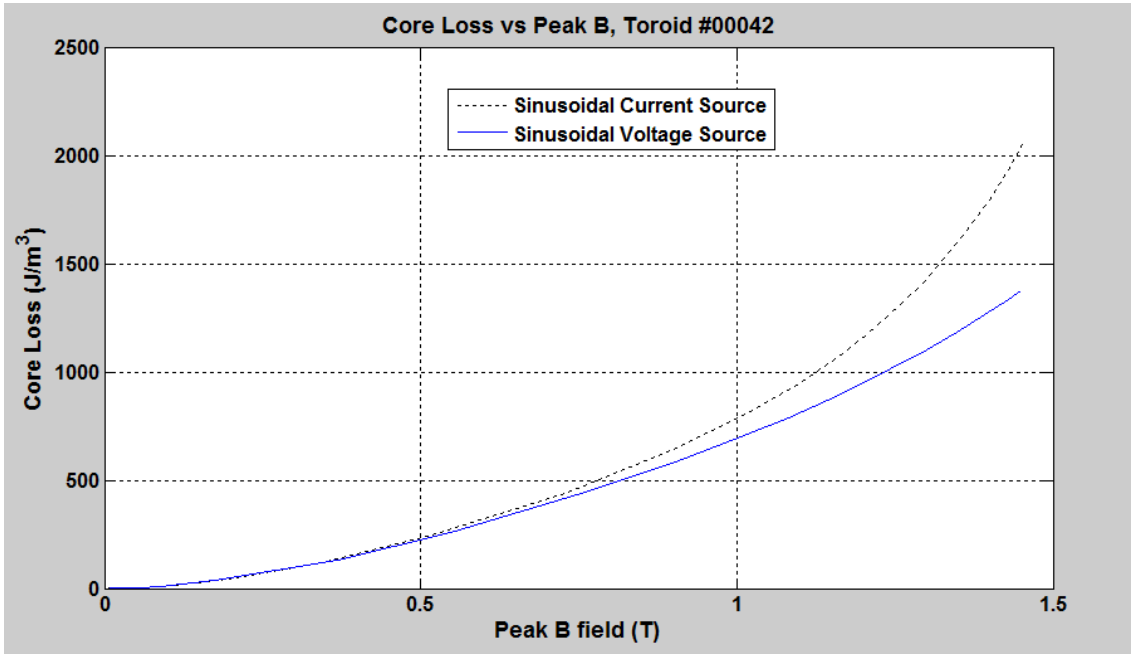

Figure 39: Core Loss (per cycle) vs. Peak Applied **B** Field, Toroid #00042

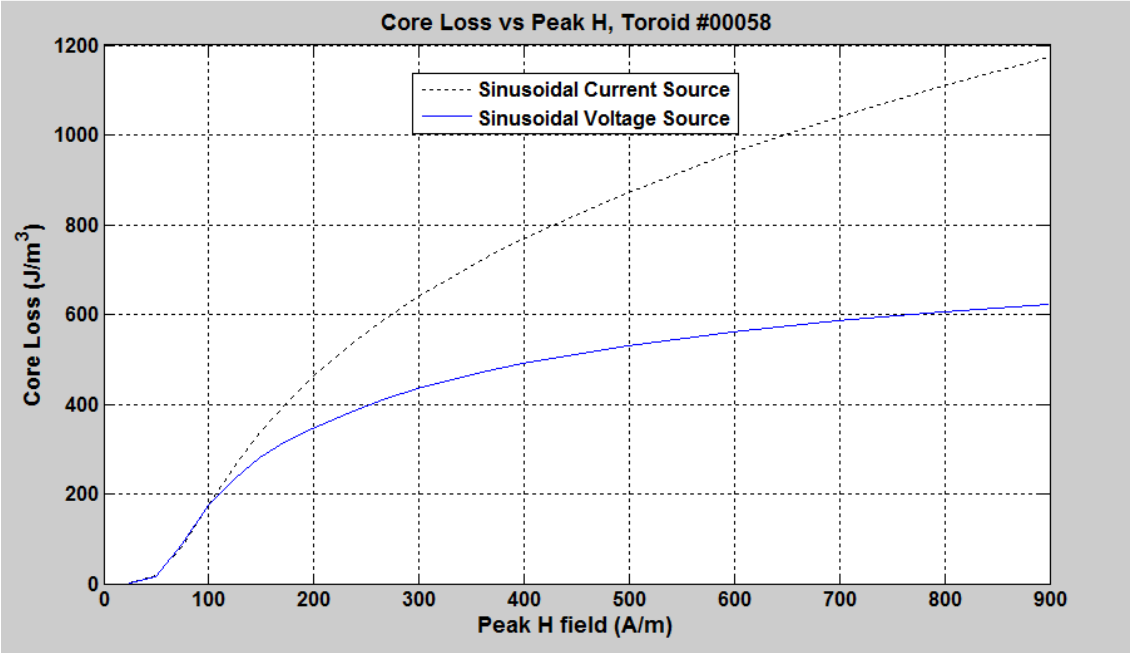

Figure 40: Core Loss (per cycle) vs. Peak Applied **H** Field, Toroid #00058

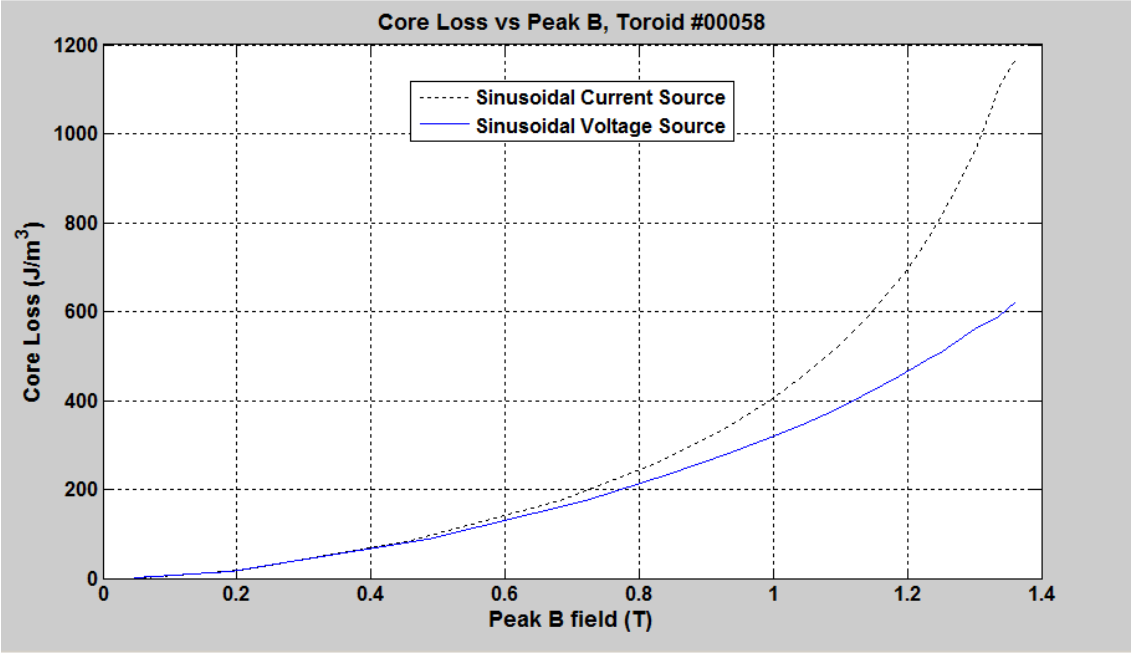

Figure 41: Loss (per cycle) vs. Peak Applied **B** Field, Toroid #00058

Figure 36 is the only figure in figures 36 through 41 in which it appears that a current sinusoid results in less core loss. It is important to note that, in this figure, core loss is plotted against peak applied **H** field. When core loss is plotted against peak flux density for that same sample (#00028), as in Figure 37, this discrepancy goes away. Previously, in Figure 25, which plotted dynamic hysteresis loops under sinusoidal voltage and current excitation for sample #00028, it could be seen that for a certain peak applied magnetic field, this sample will reach a lower peak flux under voltage source excitation than under current source excitation, at least at peak applied field levels below about 150 A/m. However, considering that the **B** field is the only truly physical magnetic field, it is more meaningful to compare hysteresis losses as compared to maximum **B** field. When this is done, it is clear that sinusoidal voltage source excitation in these tests always results in equal or less core loss than sinusoidal current source excitation.

Chapter 5: Conclusion

Prototype pulse hysteresisgraph systems were constructed to test the magnetic properties of three toroidal samples of three different soft magnetic materials. The excitation voltage and currents were supplied by one of two circuits. The first circuit created was a derivative of the class AB amplifier design, and is used to supply a current waveform to the sample under test. This amplifier uses op-amps to bias the transistors rather than the usual resistor biasing network, giving added flexibility to the amplifier. Eight parallel stages are used. The amplifier is capable of supplying very high di/dt, up to a few hundred thousand amps per second, provided that the load is not so inductive that output voltages greater than 12 V are required.

Another circuit was created to supply a voltage source waveform to the sample under test. Using six parallel stages of OPA 544T op-amps, a very low output impedance voltage buffer was created. The voltage buffer has a very high cutoff frequency (never measured by several hundred kHz at least) and very low distortion. It is capable of supplying voltage waveforms up to 20V peak-to-peak, and currents in excess of 15 A.

Theoretical modeling was undertaken to estimate the accuracy of ideal toroid assumptions of excitation field strength. The first deviation from ideal assumptions that was examined was the effect of the toroidal windings being line currents instead of the ideal surface sheet current. Solving Biot-Savart's law with MATLAB scripts, an expected deviation of a few tenths of a percent was found, and it can be concluded that replacing the toroid windings with ideal surface sheet currents is a fairly accurate assumption.

The next effect that was examined was the reduction in excitation field strength with radius due to cylindrical spreading. Ampere's Circuital Law was used and it was found that with the toroidal geometry used in all three samples, a variation in excitation field strength of approximately +/- 8% from the value at average toroid radius should be expected at the inner and outer edge of each toroid.

The final effect causing deviation from ideal assumptions of excitation field strength that was examined was the effects of eddy currents. Eddy currents create a magnetic field

opposing any change in flux in a conductive material. Using assumptions depending on the effects of these currents being trivial led to the conclusion that the effects could *not* be considered trivial. An estimate of approximately 240 A/m for the magnitude of eddy current generated **H** fields at lamination center was found when the excitation **H** field strength was 900 A/m. It is important to note that the actual reduction in **H** field strength due to this effect should be much less due to the break down in assumptions that this field strength is trivial, and due to the fact that the eddy current field should lag the exciting field by 90 degrees.

Since the theoretical approach failed to verify that the effects of eddy currents would be trivial, an analytical approach using the finite element analysis (FEA) software COMSOL Multiphysics was used. COMSOL Multiphysics also predicted a non-trivial reduction in peak **H** field in the middle of each toroid laminate of about 70 A/m. However, COMSOL used non-physical assumptions such as linear, lossless magnetization curves. Due to this, neither approaches of estimating the reduction in applied **H** field due to eddy current generated fields can be considered any more than a rough estimate. However, both methods confirmed that eddy current effects cannot be ignored and the measured values of **B** could only represent the spatial average value of **B** within a lamination.

Experimental results of the three toroid samples tested on the hysteresisgraph system demonstrated clear and significant differences between excitation of the samples with a voltage sinusoid and excitation with a current sinusoid. Very large differences were noted between current source excitation and voltage source excitation in the amount of core loss to be expected, and it is seen that for the three samples and given peak flux density, sinusoidal voltage source excitation always results in equal or less core loss than sinusoidal current source excitation. In addition to differences in core loss, small but reproducible differences were seen magnetization curves generated under sinusoidal current source and sinusoidal voltage source excitation, especially for the #00028 toroid sample.

Explanations of these differences in loss and magnetization curves were offered based on the eddy current loss mechanism. If the assumption is made that losses are being dominated by eddy current effects, then it is shown that a square voltage excitation wave should offer the lowest losses for a given peak induction level. As a voltage sinusoid will

usually come closer to the shape of a square wave than the voltage waveform induced by a sinusoidal current excitation, then it stands to reason that a sinusoidal voltage source should almost always result in less eddy current loss than a sinusoidal current source.

Appendix A: MATLAB Script to Find Dynamic Hysteresis Loops and Core Loss

```
function BHLoopInt_7(infilestring, sample, butOrd, Wn, mancurrentscale,
manvoltscale)



Hzone_fs_tol = 0.0075;% starting tolerance for the first stage automatic
loop recognizer
Bzone_fs_tol = 0.0075;

Hzone_ss_tol = 0.000005; % starting tolerance for the second stage
automatic loop recognizer
Bzone_ss_tol = 0.000005;

%start_LoopStart = 0.02;
%loopendtol = 0.1; %tolerance on loop end for automatic loop recognizer,
use default 0.2

startindextol = 0.1; %nominally 0.1

init_index_zone = 0.05;  %what percentage of total sample to initially
skip




if sample == 28
    N = 57;  %number of turns
    R =  0.017615; %radius of torroid
    d1 = 0.000914; %dimension 1 of torroid
    d2 = 0.002820; %dimension 2 of torroid
end
if sample == 42
    N = 44;    %number of turns
    R =  0.017622; %radius of torroid
    d1 = 0.000892; %dimension 1 of torroid
    d2 = 0.002857; %dimension 2 of torroid

end

if sample == 58
    N = 50;    %number of turns
    R =  0.017622; %radius of torroid
    d1 = 0.00089; %dimension 1 of torroid
```

```
    d2 = 0.002857; %dimension 2 of torroid

end



Area = d1*d2;  %cross sectional area

txt = '.txt';
rawout = '_rawout';
out = '_out';

infilename = [infilestring txt];

rawoutfilename = [infilestring rawout txt];

outfilename = [infilestring out txt];

filestring = fileread(infilename);
str_ind = 27;
if strcmp([filestring(str_ind) filestring(str_ind+1)
filestring(str_ind+2)], '(s)')
    timescale = 1;
    str_ind = str_ind + 4;
elseif strcmp([filestring(str_ind) filestring(str_ind+1)
filestring(str_ind+2) filestring(str_ind+3)], '(ms)')
    timescale = 1e-3;
    str_ind = str_ind + 5;
end
if strcmp([filestring(str_ind) filestring(str_ind+1)
filestring(str_ind+2)], '(V)')
    currentscale = 1;
    str_ind = str_ind + 4;
elseif strcmp([filestring(str_ind) filestring(str_ind+1)
filestring(str_ind+2) filestring(str_ind+3)], '(mV)')
    currentscale = 1e-3;
    str_ind = str_ind + 5;
end

if strcmp([filestring(str_ind) filestring(str_ind+1)
filestring(str_ind+2)], '(V)')
    voltagescale = 1;
    str_ind = str_ind + 3;
elseif strcmp([filestring(str_ind) filestring(str_ind+1)
filestring(str_ind+2) filestring(str_ind+3)], '(mV)')
    voltagescale = 1e-3;
    str_ind = str_ind + 4;
end
```

```
while ((strcmp(filestring(str_ind), '-'))==false) &&
((strcmp(filestring(str_ind), '0'))==false) &&
((strcmp(filestring(str_ind), '1'))==false) &&
((strcmp(filestring(str_ind), '2'))==false) &&
((strcmp(filestring(str_ind), '3'))==false) &&
((strcmp(filestring(str_ind), '4'))==false) &&
((strcmp(filestring(str_ind), '5'))==false) &&
((strcmp(filestring(str_ind), '6'))==false) &&
((strcmp(filestring(str_ind), '7'))==false) &&
((strcmp(filestring(str_ind), '8'))==false) &&
((strcmp(filestring(str_ind), '9'))==false)
    str_ind =  str_ind + 1;
end

newfilestring = filestring(str_ind:size(filestring,2));
tempfid = fopen('temp_data.txt', 'w');
fprintf(tempfid, '%s', newfilestring);
fclose(tempfid);




ITV = dlmread('temp_data.txt'); %matrix ITV stores I (current), T (time),
V (voltage)
delete('temp_data.txt');

I = 1:size(ITV, 1);
T = 1:size(ITV, 1);
V = 1:size(ITV, 1);
B = 1:size(ITV, 1);  %initialize B array
H = 1:size(ITV, 1); %initialize H array

indexarray = 1:1000; %indexarray stores values of I within tol*max value
minindexes = 1:1000; %certainly won't need 1000 points; minindexes stores
the indexes of I of the minimum values






%initialize indexarray and minindexes
for l = 1:size(indexarray,2)
    indexarray(l) = 0;
    minindexes(l) = 0;
end

currentscale = mancurrentscale*currentscale;
voltagescale = manvoltscale*voltagescale;
```

```
timescale
currentscale
voltagescale

%Dump values of I, T and V into their matrices
for ind1 = 1:size(ITV,1)
    I(ind1) = currentscale*ITV(ind1,2);
end

for ind1 = 1:size(ITV,1)
    T(ind1) = timescale*ITV(ind1,1);
end

for ind1 = 1:size(ITV,1)
    V(ind1) = voltagescale*ITV(ind1,3);
end

%-------------------------------------------------------------
% %Decimate if too big


if size(V,2)> 120000 && size(V,2)<= 240000

    V = decimate(V, 2);
    I = decimate(I, 2);
    T = decimate(T, 2);
    B = decimate(B, 2);
    H = decimate(H, 2);

elseif size(V,2) > 240000 && size(V,2)<= 480000
    V = decimate(V, 4);
    I = decimate(I, 4);
    T = decimate(T, 4);
    B = decimate(B, 4);
    H = decimate(H, 4);

elseif size(V,2) > 480000 && size(V,2)<= 960000
    V = decimate(V, 8);
    I = decimate(I, 8);
    T = decimate(T, 8);
    B = decimate(B, 8);
    H = decimate(H, 8);

elseif size(V,2) > 960000
    V = decimate(V, 16);
    I = decimate(I, 16);
    T = decimate(T, 16);
    B = decimate(B, 16);
    H = decimate(H, 16);
end
```

```
%lowpass filter the data

[CoeffB, CoeffA] = BUTTER(butOrd, Wn, 'low');

V = filter(CoeffB, CoeffA, V);
I = filter(CoeffB, CoeffA, I);







Btot = 0;

%Do initial integration to get max fluxes
for ind2 = 1:size(V, 2)

    if ind2 == 1
        Btot = T(1)*V(1);
    else
        Btot = Btot + (T(ind2)-T(ind2-1))*V(ind2);
    end
    B(ind2) = (1/(Area*N))*Btot; %divide Btot by area to get the actual B
end
    %make full H array
    H = (N/(2*pi*R)).*I;



[maxB, maxBind] = max(B);
[minB, minBind] = min(B);



%-------------------------------------------------------------
%integrate and find loop until offset is low
Bdiff = 1e6; %just a really huge number
Voffset = 0;
loopcount = 0;
while (abs(Bdiff) > abs((maxB-minB)*0.00001)) && (loopcount < 5)


    close all

    Btot = 0;
```

```
    %integrate V to get flux
    for ind2 = 1:size(V, 2)

        if ind2 == 1
            Btot = (1/(Area*N))*T(1)*(V(1) + Voffset);
        else
            Btot = Btot + (1/(Area*N))*(T(ind2)-T(ind2-1))*(V(ind2) +
Voffset);
        end
        B(ind2) = Btot;

    end

    plot(H, B)

    figure

    %Get maxes and mins of I and "B"
    [maxH, maxHind] = max(H);
    [minH, minHind] = min(H);

    [maxB, maxBind] = max(B);
    [minB, minBind] = min(B);

    %-----------------------------------------------------------------
    adjustfactor = maxH/(maxH - minH);


    adjustB = adjustfactor*(maxB-minB) - maxB;
     %adjusts the B curve so it's properly centered
    for ind3 = 1:size(B, 2)

        B(ind3) = B(ind3) + adjustB;
    end
    %-----------------------------------------------------------------

    %rest the maxes and mins for H and B
    [maxH, maxHind] = max(H);
    [minH, minHind] = min(H);

    [maxB, maxBind] = max(B);
    [minB, minBind] = min(B);

    Hzone_fs = (maxH-minH)*Hzone_fs_tol;
    Bzone_fs = (maxB-minB)*Bzone_fs_tol;

    Hzone_ss = (maxH-minH)*Hzone_ss_tol;
    Bzone_ss = (maxB-minB)*Bzone_ss_tol;
    Hzone_ss_start = Hzone_ss;
```

```
    %set starting b index, b index follows along the loop till loop
complete
    start_index =  floor(init_index_zone*size(H,2));




    after_peak_found = false;
    peak_found = false;
    start_eval = false;

    if abs(maxB) > abs(minB)
        while start_index < 0.3*size(B,2) && (after_peak_found == false)
            if abs(B(start_index)) < 0.15*abs(maxB-minB)
                start_eval = true;
            end

            if (abs(B(start_index)) > abs(0.85*maxB)) && (peak_found ==
false) && (start_eval == true)
                peak_found = true;
            end
            if (peak_found == true) && (abs(B(start_index)) <
abs(0.80*maxB))
                after_peak_found = true;
            end
            start_index = start_index + 1;
        end
    else
        while start_index < 0.5*size(B,2) && (after_peak_found == false)

            if abs(B(start_index)) < 0.15*abs(maxB-minB)
                start_eval = true;
            end

            if (abs(B(start_index)) > abs(0.85*minB)) && (peak_found ==
false) && (start_eval == true)
                peak_found = true;
            end
            if (peak_found == true) && (abs(B(start_index)) <
abs(0.80*minB))
                after_peak_found = true;
            end
            start_index = start_index + 1;
        end
    end


    %start_index should now be index of B where it is just after a peak
```

```
    b =  start_index + floor(startindextol*size(H,2));

    loopfound = 0;

    while (loopfound == 0)&&(Hzone_fs <= (maxH-minH)*0.15)

        if (b > size(H,2))
            b =  start_index + floor(startindextol*size(H,2));
            Hzone_fs = Hzone_fs + 0.5*(maxH-minH)*Hzone_fs_tol;
            Bzone_fs = Bzone_fs + 0.5*(maxB-minB)*Bzone_fs_tol;
        end

        if (abs(B(b) - B(start_index)) <= Bzone_fs)&&(abs(H(b) -
H(start_index)) <= Hzone_fs)
            'first stage loopfound'
            loopfound = 1;

        end
        b = b + 1;
    end
    b = b - 1;

    %First stage results
    if (floor((b-start_index)*0.15) + b) <= size(B,2)
    fs_stop_index = (floor((b-start_index)*0.15) + b);

    else
        fs_stop_index = size(B,2);
    end


    fs_B = B(start_index:fs_stop_index);

    fs_H = H(start_index:fs_stop_index);



    %Now start second stage
    b =  start_index + floor(0.2*size(fs_H,2));


    loopfound = 0;
```

```
    while (loopfound == 0)&&(Hzone_ss <= (maxH-minH)*0.15)

        if (b > fs_stop_index)
            %reset if b gets too big
            b =  start_index + floor(0.2*size(fs_H,2));
            Hzone_ss = Hzone_ss + 0.5*(maxH-minH)*Hzone_ss_tol;
            Bzone_ss = Bzone_ss + 0.5*(maxB-minB)*Bzone_ss_tol;
        end

        if (abs(B(b) - B(start_index)) <= Bzone_ss)&&(abs(H(b) -
H(start_index)) <= Hzone_ss)
            'second stage loopfound'
            loopfound = 1;

        end
        b = b + 1;
    end
    b = b - 1;




    %b contains index of final point in loop
    finalB = B(start_index:b);
    finalH = H(start_index:b);
    %------------------------
    %get/show voltage, current, time, electrical power, electrical energy
    finalT = T(start_index:b);
    finalI = I(start_index:b);
    finalV = V(start_index:b);




    final_index = size(finalB,2);

    Bdiff = finalB(1) - finalB(final_index);

    Vcorrection = (Area*N)*Bdiff/(finalT(final_index) - finalT(1));



    randnum1 = randn(1);
    rand_factor = (15 + randnum1)/15 ;

    Voffset = Voffset*rand_factor + Vcorrection +
0.1*randn(1)*Vcorrection;
```

```
    %randnum1 = randn(1);
    %rand_factor = (10 + randnum1)/10 ;

   % Voffset = Voffset*rand_factor + Vcorrection +
0.2*randn(1)*Vcorrection;

    %one more time for the beginning of the loop
    [maxB, maxBind] = max(B);
    [minB, minBind] = min(B);
%'Bdiff'
%Bdiff
%'abs((maxB-minB)*0.00001)'
%abs((maxB-minB)*0.00001)

plot(finalH, finalB)

loopcount = loopcount + 1;


end


Voffset_orig_est = Voffset;
%-------------------------------------------------------------------------
-
%Now, we have an approximate value of Voffset




%Create array of Voffset values from 0.1 to 10X estimated

for Voff_ind = 1:50
    Voff_array(Voff_ind) = Voffset - 2.5*Voffset + 0.1*Voff_ind*Voffset;
end


close all
size(Voff_array, 2)
for y = 1:size(Voff_array, 2)
    Btot = 0;

    %integrate V to get flux
    for ind2 = 1:size(V, 2)

        if ind2 == 1
            Btot = (1/(Area*N))*T(1)*(V(1) + Voffset);
        else
```

```
            Btot = Btot + (1/(Area*N))*(T(ind2)-T(ind2-1))*(V(ind2) +
Voff_array(y));
        end
        B(ind2) = Btot;

    end

    figure
    plot(H, B)
    %for waste_time = 1:2e6
   % end

    cor_start_ind =  floor(init_index_zone*size(H,2)); %where to start
correlation
    loop_length = b-start_index; %total length of the loop

    cor_array = 1:loop_length;

    %fill cor_array with zeros
    cor_array_ind = 1;
    while cor_array_ind <= size(cor_array,2)
        cor_array(cor_array_ind) = 0;
        cor_array_ind = cor_array_ind + 1;
    end

    %add up all the differences for each point
    for cor_ind = 0:(loop_length-1)

        cor_mult = 1;
        while (cor_start_ind + cor_ind  + cor_mult*loop_length) <=
size(B,2)

            cor_array(cor_ind + 1) = cor_array(cor_ind + 1) +
abs(B(cor_start_ind + cor_ind) - B(cor_start_ind + cor_ind  +
cor_mult*loop_length));

            cor_mult = cor_mult + 1;
        end

    end
    %now add up all the elements
    cor_array_ind = 1;
    correlation_score = 0;
    while cor_array_ind <= size(cor_array,2)
        correlation_score = correlation_score + cor_array(cor_array_ind);
        cor_array_ind = cor_array_ind + 1;
    end
    %show the correlation score:
    correlation_score
    cor_score(y) = correlation_score;
```

```
    %tmpresp = input('Continue to next? (y/n)', 's');

end

[min_cor_score, min_cor_score_ind] = min(cor_score);
'min_cor_score_ind'
min_cor_score_ind

Voffset = Voff_array(min_cor_score_ind);

'Size of Voffset compared to original estimate'
Voffset/Voffset_orig_est

Btot = 0;
%integrate V to get flux
 for ind2 = 1:size(V, 2)

     if ind2 == 1
         Btot = (1/(Area*N))*T(1)*(V(1) + Voffset);
     else
         Btot = Btot + (1/(Area*N))*(T(ind2)-T(ind2-1))*(V(ind2) +
Voffset);
     end
     B(ind2) = Btot;

 end

%-----------------------------------------------------------------------
%NOW, do final integration with appropriate Voffset



 %Get maxes and mins of I and "B"
    [maxH, maxHind] = max(H);
    [minH, minHind] = min(H);

    [maxB, maxBind] = max(B);
    [minB, minBind] = min(B);

    %-----------------------------------------------------------------------
    adjustfactor = maxH/(maxH - minH);


    adjustB = adjustfactor*(maxB-minB) - maxB;
     %adjusts the B curve so it's properly centered
    for ind3 = 1:size(B, 2)

        B(ind3) = B(ind3) + adjustB;
```

```
    end
    %-------------------------------------------------------------

    %rest the maxes and mins for H and B
    [maxH, maxHind] = max(H);
    [minH, minHind] = min(H);

    [maxB, maxBind] = max(B);
    [minB, minBind] = min(B);

    Hzone_fs = (maxH-minH)*Hzone_fs_tol;
    Bzone_fs = (maxB-minB)*Bzone_fs_tol;

    Hzone_ss = (maxH-minH)*Hzone_ss_tol;
    Bzone_ss = (maxB-minB)*Bzone_ss_tol;
    Hzone_ss_start = Hzone_ss;

    %set starting b index, b index follows along the loop till loop
complete
    start_index =  floor(init_index_zone*size(H,2));


    after_peak_found = false;
    peak_found = false;
    start_eval = false;

    if abs(maxB) > abs(minB)
        while start_index < 0.3*size(B,2) && (after_peak_found == false)
            if abs(B(start_index)) < 0.15*abs(maxB-minB)
                start_eval = true;
            end

            if (abs(B(start_index)) > abs(0.85*maxB)) && (peak_found ==
false) && (start_eval == true)
                peak_found = true;
            end
            if (peak_found == true) && (abs(B(start_index)) <
abs(0.80*maxB))
                after_peak_found = true;
            end
            start_index = start_index + 1;
        end
    else
        while start_index < 0.5*size(B,2) && (after_peak_found == false)

            if abs(B(start_index)) < 0.15*abs(maxB-minB)
                start_eval = true;
            end
```

```
            if (abs(B(start_index)) > abs(0.85*minB)) && (peak_found ==
false) && (start_eval == true)
                peak_found = true;
            end
            if (peak_found == true) && (abs(B(start_index)) <
abs(0.80*minB))
                after_peak_found = true;
            end
            start_index = start_index + 1;
        end
    end


    %start_index should now be index of B where it is just after a peak




    b =  start_index + floor(startindextol*size(H,2));

    loopfound = 0;

    while (loopfound == 0)&&(Hzone_fs <= (maxH-minH)*0.15)

        if (b > size(H,2))
            b =  start_index + floor(startindextol*size(H,2));
            Hzone_fs = Hzone_fs + 0.5*(maxH-minH)*Hzone_fs_tol;
            Bzone_fs = Bzone_fs + 0.5*(maxB-minB)*Bzone_fs_tol;
        end

        if (abs(B(b) - B(start_index)) <= Bzone_fs)&&(abs(H(b) -
H(start_index)) <= Hzone_fs)
            'first stage loopfound'
            loopfound = 1;

        end
        b = b + 1;
    end
    b = b - 1;

    %First stage results
    if (floor((b-start_index)*0.15) + b) <= size(B,2)
    fs_stop_index = (floor((b-start_index)*0.15) + b);

    else
        fs_stop_index = size(B,2);
    end
```

```
    fs_B = B(start_index:fs_stop_index);

    fs_H = H(start_index:fs_stop_index);



    %Now start second stage
    b =  start_index + floor(0.2*size(fs_H,2));


    loopfound = 0;

    while (loopfound == 0)&&(Hzone_ss <= (maxH-minH)*0.15)

        if (b > fs_stop_index)
            %reset if b gets too big
            b =  start_index + floor(0.2*size(fs_H,2));
            Hzone_ss = Hzone_ss + 0.5*(maxH-minH)*Hzone_ss_tol;
            Bzone_ss = Bzone_ss + 0.5*(maxB-minB)*Bzone_ss_tol;
        end

        if (abs(B(b) - B(start_index)) <= Bzone_ss)&&(abs(H(b) -
H(start_index)) <= Hzone_ss)
            'second stage loopfound'
            loopfound = 1;

        end
        b = b + 1;
    end
    b = b - 1;




    %b contains index of final point in loop
    finalB = B(start_index:b);
    finalH = H(start_index:b);
    %------------------------
    %get/show voltage, current, time, electrical power, electrical energy
    finalT = T(start_index:b);
    finalI = I(start_index:b);
    finalV = V(start_index:b);



   close all
   plot(H, B)
```

```
   figure



for l = 1:size(finalB, 2)
    BH(l, 1) = finalB(l);
    BH(l, 2) = finalH(l);
end



%Calculate loss mathematically
loss = 0;
rawpowerloss = 0;


dt = finalT(2) - finalT(1);
for index = start_index:b

    loss = 1/(2*pi*R*Area)*I(index)*V(index)*dt + loss;
    rawpowerloss = I(index)*V(index)*dt + rawpowerloss;
        if index ~= 1

            dt = T(index) - T(index - 1);
        end
end
T = finalT(size(finalT,2)) - finalT(1);
T
rawpowerloss = rawpowerloss/T;

loss

rawpowerloss

%-------------------------------------------------------
%Center up B
centerHtol = (maxH - minH)*0.005;
HminInds = 1:100; %should only need 1 and 2
ind1 = 1;
g = 1;
while g <= size(finalB, 2)
    curH = abs(finalH(g));
    if curH <centerHtol
        HminInds(ind1) = g;
        ind1 = ind1 + 1;
        g = g + floor(size(finalB, 2)*0.1);
    end
    g = g + 1;
end
finalBcrossH1 = finalB(HminInds(1));
```

```
finalBcrossH2 = finalB(HminInds(2));

Badj2= (abs(finalBcrossH1) - abs(finalBcrossH2))/2;

if finalBcrossH1 > 0
    for e = 1:size(finalB, 2)
       finalB(e) = finalB(e) - Badj2;

    end
else

     for e = 1:size(finalB, 2)
     finalB(e) = finalB(e) + Badj2;

     end
end

%-----------------------------------------------------------------
%output the raw data
fid = fopen(rawoutfilename,'wt');
BHraw = [finalB; finalH;];
plot(finalH, finalB)
fprintf(fid,'%12.4f  %12.4f\n', BHraw );
fclose(fid);



%-----------------------------------------------------------



%-------------------------------------------------------
%output data to file

BHdata = [finalH; finalB; finalT; finalI; finalV;];

fid = fopen(outfilename,'wt');
fprintf(fid,'Number of turns = %6.1f\n', N);
fprintf(fid,'Radius of toriod = %6.8f\n', R);
fprintf(fid,'Cross section dimension 1 = %6.8f\n', d1);
fprintf(fid,'Cross section dimension 2 = %6.8f\n', d2);
fprintf(fid,'Loss (J/m^3) calculated mathematically = %6.4f\n', loss);
fprintf(fid,'First column: H, Second column: B, Third column: time, Forth
column: I, Fifth Column: V\n');
fprintf(fid,'%12.4f  %12.4f  %12.8f  %12.4f  %12.4f\n', BHdata);
fclose(fid);

%Waste some time
figure
for waste_time = 1:2e8
```

```
end
% IV = dlmread('40_CC_IV.txt');
% for ind1 = 1:size(IV,1)
%     I_2(ind1) =IV(ind1,1);
% end
%
% for ind1 = 1:size(IV,1)
%     V_2(ind1) = IV(ind1,2);
% end
% plot(finalI, finalV, I_2, V_2)
end
```

Apendeix B: MATLAB Script for Simulating H field Created By Discrete Wires

```
Iw = 2;
elements = 25
'elements per mm'
grdspc = 0.001/elements;
ro = 0.017615;
tau = 2*pi*ro/57; %For #00028
h = 0.004;
w = 0.006;
C = 2*h + 2*w;

line_els = 20;
add_units = 10;  %add this many unit cells to either end


rsx = 0:line_els;
rsy = 0:line_els;
rsz = 0:line_els;
for l = 1:size(rsx,2)
    rsx(l) = 0;
    rsz(l) = rsz(l)/(size(rsz,2) - 1);
    rsz(l) = rsz(l)*h*tau/C;
    rsy(l) = C/tau*rsz(l);
end

tx = 0:line_els;
ty = 0:line_els;
tz = 0:line_els;
for l = 1:size(tx,2)
    ty(l) = h;
    tz(l) = tz(l)/(size(tz,2) - 1);
    tz(l) = tz(l)*w*tau/C;
    tx(l) = C/tau*tz(l);
    tz(l) = tz(l) + + h*tau/C;
end


lsx = 0:line_els;
lsy = 0:line_els;
lsz = 0:line_els;
for l = 1:size(lsx,2)
    lsx(l) = w;
    lsz(l) = lsz(l)/(size(lsz,2) - 1);
    lsz(l) = lsz(l)*h*tau/C;
    lsy(l) = -C/tau*lsz(l) + h;
    lsz(l) = lsz(l) + + (h + w)*tau/C;
end
```

```
bx = 0:line_els;
by = 0:line_els;
bz = 0:line_els;
for l = 1:size(bx,2)
    by(l) = 0;
    bz(l) = bz(l)/(size(bz,2) - 1);
    bz(l) = bz(l)*w*tau/C;
    bx(l) = -C/tau*bz(l) + w;
    bz(l) = bz(l) +  + (2*h + w)*tau/C;
end

subwire_x = 1:(4*line_els);
subwire_y = 1:(4*line_els);
subwire_z = 1:(4*line_els);
subcounter1 = 1;
subcounter2 = 1;
subcounter3 = 1;
l = 1;
for l = 1:(4*line_els)
    if (l <= (line_els))
        subwire_x(l) = rsx(l);
        subwire_y(l) = rsy(l);
        subwire_z(l) = rsz(l);

    end
    if (l <= line_els*2)&&(l > line_els)
        subwire_x(l) = tx(subcounter1);
        subwire_y(l) = ty(subcounter1);
        subwire_z(l) = tz(subcounter1);
        subcounter1 = subcounter1 + 1;

    end
    if (l <= line_els*3)&&(l > line_els*2)
        subwire_x(l) = lsx(subcounter2);
        subwire_y(l) = lsy(subcounter2);
        subwire_z(l) = lsz(subcounter2);
        subcounter2 = subcounter2 + 1;

    end
    if (l <= line_els*4)&&(l > line_els*3)
        subwire_x(l) = bx(subcounter3);
        subwire_y(l) = by(subcounter3);
        subwire_z(l) = bz(subcounter3);
        subcounter3 = subcounter3 + 1;

    end



end
wire_x = 1:((add_units*2 + 1)*(size(subwire_x, 2)));  %wire
```

```
wire_y = 1:size(wire_x, 2);  %wire
wire_z = 1:size(wire_x, 2);  %wire

repeatcounter = 1;
wirespacer = -1*add_units;
k = 1;
while k <= size(wire_x,2) %add unit cells
    if repeatcounter <= size(subwire_x,2)
        wire_x(k) = subwire_x(repeatcounter);
        wire_y(k) = subwire_y(repeatcounter);
        wire_z(k) = subwire_z(repeatcounter) + wirespacer*tau;
        repeatcounter = repeatcounter + 1;
        k = k + 1;
    else
        repeatcounter = 1;
        wirespacer = wirespacer + 1;

    end

end

close all

%plot3(rsx, rsy, rsz, 'g', tx, ty, tz, 'b', lsx, lsy, lsz, 'r', bx, by,
bz, 'k')
%figure
plot3(wire_x, wire_y, wire_z)
figure


%-------------------------------------------
%Make 3D mesh:
%z goes from 0 to tau
%x goes from + 1.5mm to +4.5 mm
%y goes from +1.5mm to + 2.5mm
ztot = 0;
ztotcntr = 0;
while ztot < tau
   ztot = ztot + grdspc;
   ztotcntr = ztotcntr + 1;
end
xtot = 0;
xtotcntr = 0;
while xtot < 0.003
   xtot = xtot + grdspc;
   xtotcntr = xtotcntr + 1;
end
ytot = 0;
ytotcntr = 0;
while ytot < 0.001
   ytot = ytot + grdspc;
```

```
   ytotcntr = ytotcntr + 1;
end

[X,Y,Z] = meshgrid(0:(xtotcntr-1), 0:(ytotcntr-1), 0:(ztotcntr-1));
xtotcntr
ytotcntr
ztotcntr
size(X)
pause
X = X.*grdspc;
Y = Y.*grdspc;
Z = Z.*grdspc;
Hx = X;  %just initialize them to the right size
Hy = Y;
Hz = Z;
Hmag = X;
for cz = 1:size(Hx,3)
    for cy = 1:size(Hx,1)
        for cx = 1:size(Hx, 2)
        Hx(cy, cx, cz) = 0;
        Hy(cy, cx, cz) = 0;
        Hz(cy, cx, cz) = 0;
        Hmag(cy, cx, cz) = 0;
        end
    end
end


for x_ind = 1:size(X, 2)
    for y_ind = 1:size(X,1)
        for z_ind = 1:size(X,3)
            X(y_ind, x_ind, z_ind) = X(y_ind, x_ind, z_ind) + 0.0015;
            Y(y_ind, x_ind, z_ind) = Y(y_ind, x_ind, z_ind) + 0.0015;
        end
    end
end



%-------------------------------------------------------------------------

endpnt_ind = 2;
startpnt_ind = 1;
%--------------------------------------
%for progress updates
estimate = ztotcntr*xtotcntr*ytotcntr*size(wire_x,2);  %how many
calculations of dH will be done
percentcntr = 0;
calcs = 1;
%--------------------------------------
```

```
while endpnt_ind <= size(wire_x,2)
    for x_ind = 1:size(X, 2)
        for y_ind = 1:size(X,1)
            for z_ind = 1:size(X,3)
                xp = X(y_ind,x_ind,z_ind); %x coord of point within domain
                yp = Y(y_ind,x_ind,z_ind); %y coord of point within domain
                zp = Z(y_ind,x_ind,z_ind);
                dLx = wire_x(endpnt_ind) - wire_x(startpnt_ind);
                dLy = wire_y(endpnt_ind) - wire_y(startpnt_ind);
                dLz = wire_z(endpnt_ind) - wire_z(startpnt_ind);
                dL = [dLx dLy dLz];
                %Approximate R as being from start of dL to point
                xmid = (wire_x(startpnt_ind) + wire_x(endpnt_ind))/2;
                ymid = (wire_y(startpnt_ind) + wire_y(endpnt_ind))/2;
                zmid = (wire_z(startpnt_ind) + wire_z(endpnt_ind))/2;
                Rx = xp - xmid;
                Ry = yp - ymid;
                Rz = zp - zmid;
                R = (Rx^2 + Ry^2 + Rz^2)^0.5;
                %unit vector
                aR = [Rx/((Rx^2 + Ry^2 + Rz^2)^0.5) Ry/((Rx^2 + Ry^2 +
Rz^2)^0.5) Rz/((Rx^2 + Ry^2 + Rz^2)^0.5)];
                C = Iw/(4*pi*R^2);
                crossprod = cross(dL, aR);
                dH = crossprod.*C;
                Hx(y_ind,x_ind,z_ind) = Hx(y_ind,x_ind,z_ind) + dH(1);
                Hy(y_ind,x_ind,z_ind) = Hy(y_ind,x_ind,z_ind) + dH(2);
                Hz(y_ind,x_ind,z_ind) = Hz(y_ind,x_ind,z_ind) + dH(3);

                steps = floor(estimate/1000);
                if mod(calcs, steps) == 0
                    percentcntr = percentcntr + 0.1;
                    percentcntr
                end

                calcs = calcs + 1;




            end

        end
    end



    endpnt_ind = endpnt_ind + 1;
    startpnt_ind = startpnt_ind + 1;
end
```

```
for x_ind = 1:size(X, 2)
    for y_ind = 1:size(X,1)
        for z_ind = 1:size(X,3)
            Hmag(y_ind,x_ind,z_ind)  = (Hx(y_ind,x_ind,z_ind)^2 +
Hy(y_ind,x_ind,z_ind)^2 + Hz(y_ind,x_ind,z_ind)^2)^0.5;
        end
    end
end


%0.1*ytotcntr
for x_ind = 1:size(X, 2)
    for z_ind = 1:size(X,3)
            H01(z_ind, x_ind)  = Hmag(floor(ytotcntr*0.15), x_ind, z_ind);

    end
end

for x_ind = 1:size(X, 2)
    for z_ind = 1:size(X,3)
            X01(z_ind, x_ind)  = X(floor(ytotcntr*0.15), x_ind, z_ind);
            Z01(z_ind, x_ind)  = Z(floor(ytotcntr*0.15), x_ind, z_ind);
    end
end
'floor(ytotcntr*0.15) value'
Y(floor(ytotcntr*0.15),1,1)
'floor(ytotcntr*0.35) value'
Y(floor(ytotcntr*0.35),1,1)
'floor(ytotcntr*0.55) value'
Y(floor(ytotcntr*0.55),1,1)
'floor(ytotcntr*0.75) value'
Y(floor(ytotcntr*0.75),1,1)
'floor(ytotcntr*0.95) value'
Y(floor(ytotcntr*0.95),1,1)
%0.3*ytotcntr
for x_ind = 1:size(X, 2)
    for z_ind = 1:size(X,3)
            H03(z_ind, x_ind)  = Hmag(floor(ytotcntr*0.35), x_ind, z_ind);

    end
end

for x_ind = 1:size(X, 2)
    for z_ind = 1:size(X,3)
            X03(z_ind, x_ind)  = X(floor(ytotcntr*0.35), x_ind, z_ind);
            Z03(z_ind, x_ind)  = Z(floor(ytotcntr*0.35), x_ind, z_ind);
    end
end
```

```
%0.5*ytotcntr
for x_ind = 1:size(X, 2)
    for z_ind = 1:size(X,3)
            H05(z_ind, x_ind)  = Hmag(floor(ytotcntr*0.55), x_ind, z_ind);

    end
end

for x_ind = 1:size(X, 2)
    for z_ind = 1:size(X,3)
            X05(z_ind, x_ind)  = X(floor(ytotcntr*0.55), x_ind, z_ind);
            Z05(z_ind, x_ind)  = Z(floor(ytotcntr*0.55), x_ind, z_ind);
    end
end


%0.7*ytotcntr
for x_ind = 1:size(X, 2)
    for z_ind = 1:size(X,3)
            H07(z_ind, x_ind)  = Hmag(floor(ytotcntr*0.75), x_ind, z_ind);

    end
end

for x_ind = 1:size(X, 2)
    for z_ind = 1:size(X,3)
            X07(z_ind, x_ind)  = X(floor(ytotcntr*0.75), x_ind, z_ind);
            Z07(z_ind, x_ind)  = Z(floor(ytotcntr*0.75), x_ind, z_ind);
    end
end

%0.9*ytotcntr
for x_ind = 1:size(X, 2)
    for z_ind = 1:size(X,3)
            H09(z_ind, x_ind)  = Hmag(floor(ytotcntr*0.95), x_ind, z_ind);

    end
end

for x_ind = 1:size(X, 2)
    for z_ind = 1:size(X,3)
            X09(z_ind, x_ind)  = X(floor(ytotcntr*0.95), x_ind, z_ind);
            Z09(z_ind, x_ind)  = Z(floor(ytotcntr*0.95), x_ind, z_ind);
    end
end


surf(Z01, X01, H01)
title('H @ y = 0.1mm from bottom toroid surface')
%hold on
```

```
%plot3(wire_x, wire_z, wire_y)
%hold off
figure
surf(Z03, X03, H03)
title('H @ y = 0.3mm from bottom toroid surface')
figure
surf(Z05, X05, H05)
title('H @ y = 0.5mm from bottom toroid surface (at center)')
figure
surf(Z07, X07, H07)
title('H @ y = 0.7mm from bottom toroid surface (0.3mm below top
surface)')
figure
surf(Z09, X09, H09)
title('H @ y = 0.9mm from bottom toroid surface (0.1mm below top
surface)')
```

References

[1] P. C. Sen, *Principles of Electric Machines and Power Electronics.* John Wiley & Sons, 1997, pp. 16-22.

[2] W. H. Hayt, *Engineering Electromagnetics*. McGraw-Hill, 1981, p. 252.

[3] D. M. Zhang and C. F. Foo, "A simple method to estimate the magnetic field distribution due to current-carrying winding in toroidal core and its influence on the measurement of complex permeability and core losses," *Journal of Magnetism and Magnetic Materials,* vol. 191, 1999, pp. 189-198.

[4] A. T. Wilder, J. J. Tatarchuk, J. C. Soric, "Soft magnetic material response with rate of field," *IET Science, Measurement, and Technology*, submitted for publication.

[5] *IEEE Standard for Test Procedures for Magnetic Cores,* IEEE Standard 393, 1991.

[6] P. C. Sen, *Principles of Electric Machines and Power Electronics.* John Wiley & Sons, 1997, pp. 96-101.

[7] M. Jaafar, V. Markovski, M. Elleuch, "Modelling of the differential permeability and the initial magnetization curve for ferromagnetic materials," in *IEEE Int. Conf. on Industrial Technology, 2004.* December 8-10, 2004, pp. 460- 465.

[8] C. Y. Leong, N. P. van der Duijn Schouten, P. D. Malliband, R. A. McMahon, "A comparison of power losses for small (< 1 kW) induction motor drives adopting squarewave and sinusoidal PWM excitation," in *Second Int. Conf. on Power Electronics, Machines and Drives, 2004.* 31 March 31- April 2, 2004, pp. 286- 290.

[9] D. Lin, T. Batan, E.F. Fuchs, W. M. Grady, "Harmonic losses of single-phase induction motors under nonsinusoidal voltages," *IEEE Trans. Energy Conversion,* vol.11, pp.273-286, June 1996.